Biophysical Journal, Volume *113*

Supplemental Information

H4 Tails Potentially Produce the Diversity in the Orientation of Two Nucleosomes

Hisashi Ishida and Hidetoshi Kono

Supporting Material

H4 tails potentially produce the diversity in the orientation of two nucleosomes

Hisashi Ishida* and Hidetoshi Kono

Molecular Modeling and Simulation Group, Department of Quantum Beam Life Science, National Institutes for Quantum and Radiological Science and Technology, 8-1-7 Umemidai, Kizugawa, Kyoto 619-0215, Japan

* Corresponding author: ishida.hisashi@qst.go.jp

Simulated Annealing in vacuum

All the MD simulations were carried out using an MD simulation program called SCUBA (1-5) with the AMBER *ff*99SB (6), *ff*99bsc0 (7) and *ff*99ions08 (8) force-fields for histones, DNAs and ions, respectively. In order to optimize the conformation of the modelled tails, simulated annealing (SA) was performed in vacuum by assuming a distance-dependent dielectric constant of 4.0*r* with the value of *r* in Ångstrom. The van der Waals interactions were evaluated with a cut-off radius of 14 Å. All atoms of the modelled tails of the two NCPs were free to move but other heavy atoms of the histones and the DNA were restrained by harmonic restraints with a force constant of 10 kcal/mol/Å^2. Non-bonded interactions were evaluated with a cut-off radius of 12 Å. A time-step of 0.5 fs was used throughout the SA. The system was heated from 0 to 800 K during the first 50 ps and was then equilibrated for 50 ps. The equilibrated system was then gradually cooled for 400 ps from 800 K to 300 K. The SA was repeated 150 times and the resulting coordinate sets were stored as possible conformations of the tails at local minimum energy regions. Each of the 150 conformations was minimized for 500 steps using steepest descent followed by 5,000 steps of conjugate gradient. Then, the 63 lowest energy structures were selected as representatives of the two NCPs with H4 tails located in different positions. Here the energy considered was the total of the internal energy of the tails and the interaction energy between the tails and the two NCPs.

MD simulations of the systems in water

After the SA, the 63 structures were each placed in an aqueous medium. Each system of the two NCPs was placed in a rectangular box ~ 140 Å × 165 Å × 215 Å with the axis of the stacking of the two NCPs in the *z*-direction. In each box, all atoms of the two NCPs were separated more than 15 Å from the lateral edge of the box and 40 Å from the top edge of the box. To neutralize the charges of each system, sodium ions were placed at positions with large negative electrostatic potential. (438 Na^+ were used for neutralization.) Moreover, sodium and chloride ions were added to each box at random positions at a concentration of 150 mM NaCl. Then ~ 135,000 TIP3P water molecules (9) were added to surround each system. In total, each system comprised ~ 460,000 atoms.

To carry out energy minimization of all the systems to alleviate unfavorable interactions between the polymers and water molecules, steepest descent was performed for 500 steps, and conjugate gradient was performed for 5,000 steps. Harmonic restraints with a force constraint of 1.0 kcal/mol/Å^2 were applied to all the heavy atoms

of the molecules. The dielectric constant used was 1.0 and the van der Waals interactions were evaluated with a cut-off radius of 9 Å. The particle-particle particle-mesh (PPPM) method (10,11) was used for the electrostatic interactions for the direct space cutoff of 9 Å. For the PPPM calculations, charge grid sizes of 144 × 160 × 216 were chosen for the two NCPs system to set charge grid spacing close to 1 Å. The charge grid was interpolated using a spline of the order of seven, while the force was evaluated using a differential operator of the order of six (11).

All the systems were equilibrated at a constant pressure of one bar and a temperature of 300 K for 5 ns. The Langevin dynamics algorithm was utilized to control the temperature and pressure of the system. The coupling times for the temperature and pressure control were both set at 2 ps^{-1}. The SHAKE algorithm (12,13) was used to constrain all the bond lengths involving hydrogen atoms. The leap-frog algorithm with a time step of 2 fs was used throughout the simulation to integrate the equations of motion. Each system was first heated from 0 K to 300 K within 1 ns during which the molecules and sodium ions were fixed with decreasing restraints and the water molecules were allowed to move. After these the restraints were removed, the system was equilibrated for 10 ns at a constant pressure of one bar and a temperature of 300 K with no restraint. Then the box size was fixed, and an adaptively biased molecular dynamics (ABMD) simulation was carried out at a constant volume for all 63 structures with different initial coordinates of the H4 tails.

Adaptively Biased Molecular dynamics (ABMD) simulation

To observe the separation of the NCPs in the two NCPs, the ABMD method (14) combined with the multiple walker method (15) was employed in SCUBA. The equations of motion used in the ABMD method are expressed as (14):

$$\begin{aligned} m_a \frac{d^2\mathbf{r}_a}{dt^2} &= \mathbf{F}_a - \frac{\partial}{\partial \mathbf{r}_a} U\left[t \mid \sigma(\mathbf{R})\right], \\ \frac{\partial U(t \mid d)}{\partial t} &= \frac{k_B T}{\tau_F} K\left[d - \sigma(\mathbf{R})\right], \end{aligned} \qquad \text{(S1)}$$

where $\mathbf{R} \equiv (\mathbf{r}_1, ..., \mathbf{r}_N)$ are the coordinates of the NCP, and N is the number of atoms in the two NCPs. d is the reaction coordinate, and $\sigma(\mathbf{R})$ is a function to give the value of the reaction coordinate. k_B is the Boltzmann constant, T is the constant temperature, τ_F is the flooding time scale, and K is the kernel which has distribution around the reaction coordinate. The first equation is for atom a, with an additional force coming from the biasing potential $U(t|d)$ with an ordinary atomic force of $\boldsymbol{F_a}$. The second equation is

the time-evolving equation of the biasing potential. Details of the ABMD algorithm used in SCUBA are given in a reference (4).

The ABMD simulations were carried out at a constant volume and a temperature of 300K for 134 ns per system (a total of 8.4 μs for all 63 systems). The value of the reaction coordinate in the initial structure was 57.2 Å, and the range of the reaction coordinate for the ABMD simulations was set at $d \geq 50.0$ Å. The resolution of the reaction coordinate, Δd, was set at 1.0 Å. The relaxation time for the free-energy profile in Eq. (S1), τ, was set at 5000 ps. The two NCPs separated from each other in many systems as shown in Fig. 2. The conformation of the NCPs was stored every 1 ps for analysis.

Umbrella sampling simulations

Theoretically, for large enough τ_F and small enough width of the kernel, $U(t|d)$ converges towards the free-energy $F(d)$ times −1 as the simulation time elapses from $t = 0$ to ∞ (14). Using τ_F with a certain finite amount of time, the biasing potential (free-energy landscape times −1) fluctuates around the free-energy during the ABMD simulation (4,14). However, the biased potential did not show any fluctuation as shown in Fig. S1(a), indicating that the convergence of the free-energy is not accomplished. Moreover, as 63 systems moved to different conformations from each other as shown in Fig. 3, the identical biasing potential in our ABMD simulation would not be appropriate to represent possible different free-energies for each system. In this study, we paid attention to some models which we observed had distinctive orientations of the NCPs in the ABMD simulation, (LEFTs 1-3, RIGHTs 1-3 and PARALLELs 1-2 as shown in Fig. 3). Instead of continuing the ABMD simulation, we carried out umbrella sampling simulations of these models to obtain their free-energies.

The weighted histogram analysis method (WHAM) (16) was used to evaluate the free-energy from the sampled trajectories in the umbrella sampling simulations. In the WHAM approach, the unbiased probability distribution $P(\mathbf{R})$ is calculated from the biased probability distribution of the sampled coordinates as:

$$P(\mathbf{R}) = \sum_{i=1}^{N_{win}} n_i(\mathbf{R}) P_i^{(b)}(\mathbf{R}) \times \left[\sum_{j=1}^{N_{win}} n_j(\mathbf{R}) \exp\left(\left[F_j - V_j(\mathbf{R}) \right] / k_B T \right) \right]^{-1}, \qquad \text{(S2)}$$

where $\mathbf{R}$ is the atomic coordinates, N_{win} is the number of windows, $n_i(\mathbf{R})$ is the number of data points in the i-th window, $P_i^{(b)}(\mathbf{R})$ is a biased probability from the raw data obtained in the umbrella sampling simulation, $V_j(\mathbf{R})$ is the biasing potential in the j-th window, k_B is the Boltzmann constant, and T is the constant temperature. In this study,

$V_j(\mathbf{R})$ was selected to be the sum of a harmonic potential and the ABMD biasing potential in the final stage of the ABMD simulation, which has the form:

$$V_i(\mathbf{R}) = k_i\left(d(\mathbf{R}) - d_i^{\mathrm{fix}}\right)^2 + c\cdot\left(U_{abmd}\left(d(\mathbf{R})\right) - U_{abmd}\left(d_0\right)\right), \qquad \text{(S3)}$$

where $d(\mathbf{R})$ is the umbrella sampling coordinate, which was set to be $\sigma(\mathbf{R})$. d_i^{fix} is a fixed distance to sample umbrella coordinates of $d(\mathbf{R})$ around the desired position of d_i^{fix}. The initial coordinates of $\mathbf{R}$ for the i-th window were selected from the trajectories which had similar d_i^{fix} in the ABMD simulation. The values of d_i^{fix} were set from 58 Å to 110, 115 and 110 Å for LEFTs 1-3, 122, 118 and 105 Å for RIGHTs 1-3, 100 and 80 Å for PARALLELs 1-2, respectively, with intervals of 1 Å (i = 1,..., N_{win}). k_i is an arbitrary harmonic force constant, which was set at 0.2 kcal/mol/Å^2. U_{abmd} is the biasing potential at the final stage of the ABMD simulation (Fig. S1(a)). d_0 is a constant so that $U_{abmd}\left(d(\mathbf{R})\right) - U_{abmd}^0$ is zero at $d = d_0$. c is the arbitrary constant to scale U_{abmd}. If U_{abmd} were converged to the real free-energy landscape times -1, then $V_i(\mathbf{R})$ with k_i = 0.0 and c = 1.0 would let the NCPs behave like a random walk on the reaction coordinate of d. However, in an umbrella sampling simulation with c = 1.0, d monotonically drifted from the desired distance by ~ 3.0 Å on average for each window during each 10 ns (data not shown). This indicates that U_{abmd} at 134 ns overestimated the real free-energy. In contrast, using c = 0.0 shifted d from the desired position in a negative direction at $d \geq 60.0$ Å. In this study, c = 0.25 and 0.0 were used for $d > d_0$ and $d \leq d_0$ with d_0 = 60.0 Å, respectively. (More precisely, the biasing potential is expanded in terms of a third order B-spline function, and the coefficients of the B-spline function for $d \leq 60.0$ Å were set at zero. Therefore, the umbrella sampling potential is smoothly connected at d = 60.0 Å (see Fig. S1(b).) The initial atomic velocities were reset to eliminate the possibility of water convection by the separation of the NCPs during the ABMD simulation. The umbrella sampling simulation was carried out for 30 ns. The conformations of the NCPs was stored every 1 ps for analysis. The trajectory for the last 20 ns was used for the calculation of the free-energy landscape.

The coefficient F_j is defined by:

$$F_j = -k_B T \ln\left\{\sum_{\text{windows}} P(\mathbf{R})\exp\left(\left[-V_j(\mathbf{R})\right]/k_B T\right)\right\}, \quad (j = 1,\ldots N_{win}) \qquad \text{(S4)}$$

where the summation includes all the coordinates of **R** which were sampled over the total number of windows. By iterating Eqs. (S2) and (S4) to achieve self consistency (using a tolerance of 10^{-8}), the relative free-energy $F(\mathbf{R})$ at a given **R** is obtained as:

$$F(\mathbf{R}) = -k_B T \ln P(\mathbf{R}). \quad \text{(S5)}$$

To visualize the free-energy profile, the dimension of **R** in Eq. (S5) was reduced to 1 dimension by using the reaction coordinate, *d*.

The probability of the trajectories on *d*, $P(d)$, can be written as:

$$P(d) = \int P(\mathbf{R}')\delta(d - d')d\mathbf{R}', \quad \text{(S6)}$$

where $\delta(d)$ is the Dirac delta-function, and the free-energy profile in 1-dimension has the same form as Eq. (S5):

$$F(d) = -k_B T \ln P(d). \quad \text{(S7)}$$

To describe the changes in a physical quantity, *A*, such as the distance between atoms along *d*, the averaged quantity at *d*, $\bar{A}(d)$, is calculated by weighing the unbiased probability on the quantity $A(\mathbf{R})$ as:

$$\bar{A}(d) = \frac{\int A(\mathbf{R}')P(\mathbf{R}')\delta(d - d')d\mathbf{R}'}{P(d)}. \quad \text{(S8)}$$

The root mean square deviation (rmsd) from $\bar{A}(d)$ is calculated as:

$$\sqrt{\sigma^2(d)} = \sqrt{\overline{A^2}(d) - \bar{A}(d)^2} \quad \text{(S9)}$$

Umbrella sampling simulations of two NCPs without the H4 tails

To understand the role of the H4 tails, umbrella sampling simulations of two NCPs without the H4 tails were also carried out for LEFT 1, RIGHT 1 and PARALLEL 1 which had distinctive orientations of the NCP-NCP conformation. The initial atomic structure of the two NCPs without the H4 tails for each window was simply modeled by truncating the H4 tails (Ser1 to Ile 26) in the two NCPs which was used in the previous umbrella sampling simulations. To maintain the neutralization of the system, sodium ions were located at the positons of CZ atoms of Arg3, Arg17, Arg19, and Arg23, and NZ atoms of Lys5, Lys8, Lys12, Lys16, Lys20 in the H4 tails. Chloride ions were located at the positions of CG atoms of Asp24 in the H4 tails. An additional 172 × 4 water molecules were located at the positions of the other 172 × 4 heavy atoms of the four H4 tails to fill up the system. The system was minimized in the same way as

mentioned in “MD simulations of the systems in water”. Umbrella sampling simulations were carried out in the same way as mentioned in “Umbrella sampling simulations”, except for a longer simulation time of 40 ns with the last 20 ns analyzed. The arbitrary constant *c* in Eq. (S3) was set at zero for all the windows in the WHAM.

The conformational entropies of the H4 and H2A tails

The conformational entropies of the H4 and H2A tails were calculated using the quasiharmonic approximation (17) as follows:

$$S_{\mathrm{conf}} = 0.5\, k_B \ln \det [\mathbf{1}+(k_B T e^2/\hbar^2)\boldsymbol{\sigma}], \qquad \text{(S10)}$$

where *e* is *Euler*’s number, $\hbar$ is Planck’s constant divided by 2π. $\boldsymbol{\sigma} = < \boldsymbol{x}\, \boldsymbol{x}^{\mathrm{T}} >$ represents the mass-weighted covariance matrix, where $\boldsymbol{x}$ is the coordinates of the H4 $\mathrm{tail}_{1/2}$ (residues 1 to 26, 401 atoms) and the H2A $\mathrm{tail}_{1/2}$ (residues 1 to 17, 266 atoms). The trajectories in the *i*-th window of the umbrella sampling simulation where the desired position of d_i^{fix} was set in Eq. (S3) were used for the calculation of the conformational entropies to keep the number of sampled conformations the same for all d_i^{fix}. For the calculation of each covariance matrix for the H4 and H2A tails, $\boldsymbol{x}$ was best-fit in the reference coordinates. Each of the coordinates of the H4 and H2A $\mathrm{tails}_{1/2}$ in the initial structure in the *i*-th window of the umbrella sampling simulation was used as the reference coordinates for the best-fit at d_i^{fix}. (Hereafter, d_i^{fix} is referred to as d^{fix} unless it is specifically mentioned otherwise.) It should be noted that the conformational entropies calculated by the quasiharmonic approximation can be markedly overestimated because of the anharmonicity in protein dynamics (4).

SEQRES 1 I 347 DA DC DT DT DA DC DA DT DG DC DA DC DA

SEQRES 2 I 347 DG DG DA DT DG DT DA DA **DC=(Cyt22)$_1$** DC DT DG DC

SEQRES 3 I 347 DA DG DA DT DA DC DT DA DC DC DA DA DA

SEQRES 4 I 347 DA DG DT DG DT DA DT DT DT DG DG DA DA

SEQRES 5 I 347 DA DC DT DG DC DT DC DC DA **DT=(Thy62)$_1$** DC DA DA

SEQRES 6 I 347 DA DA DG DG DC DA DT DG DT DT DC DA DG

SEQRES 7 I 347 DC DT DG DG DA DT DT DC DC DA DG DC DT

SEQRES 8 I 347 DG DA DA DC DA DT DG DC DC DT DT DT DT

SEQRES 9 I 347 DG DA DT DG DG DA DG DC DA DG DT DT DT

SEQRES 10 I 347 DC DC DA DA DA DT DA DC DA DC DT DT DT

SEQRES 11 I 347 DT DG DG DT DA DG DT DA DT DC DT DG DC

SEQRES 12 I 347 DA DG DG DT DG DA DT DT DC DT DC DC DA

SEQRES 13 I 347 DG DG DG DC DG DG DC DC DA DG DT DA DC

SEQRES 14 I 347 DT DT DA DC DA DT DG DC DA DC DA DG DG

SEQRES 15 I 347 DA DT DG DT DA DA **DC=(Cyt189)$_2$** DC DT DG DC DA DG

SEQRES 16 I 347 DA DT DA DC DT DA DC DC DA DA DA DA DG

SEQRES 17 I 347 DT DG DT DA DT DT DT DG DG DA DA DA DC

SEQRES 18 I 347 DT DG DC DT DC DC DA **DT=(Thy229)$_2$** DC DA DA DA DA

SEQRES 19 I 347 DG DG DC DA DT DG DT DT DC DA DG DC DT

SEQRES 20 I 347 DG DG DA DT DT DC DC DA DG DC DT DG DA

SEQRES 21 I 347 DA DC DA DT DG DC DC DT DT DT DT DG DA

SEQRES 22 I 347 DT DG DG DA DG DC DA DG DT DT DT DC DC

SEQRES 23 I 347 DA DA DA DT DA DC DA DC DT DT DT DT DG

SEQRES 24 I 347 DG DT DA DG DT DA DT DC DT DG DC DA DG

SEQRES 25 I 347 DG DT DG DA DT DT DC DT DC DC DA DG DA

SEQRES 26 I 347 DC DT DT DA DC DA DT DG DC ~~DG DC DA DT~~

SEQRES 27 I 347 ~~DG DT DA DA DG DT DG DC DA~~

SEQRES 1 J 347 ~~DT DG DC DA DC DT DT DA DC DA DT DG DC~~

SEQRES 2 J 347 DG DC DA DT DG DT DA DA DG DT DC DT DG

SEQRES 3 J 347 DG DA DG DA DA DT DC DA DC DC DT DG DC

SEQRES 4 J 347 DA DG DA DT DA DC DT DA DC DC DA DA DA

SEQRES 5 J 347 DA DG DT DG DT DA DT DT DT DG DG DA DA

SEQRES 6 J 347 DA DC DT DG DC DT DC DC DA DT DC DA DA

SEQRES 7 J 347 DA DA DG DG DC DA DT DG DT DT DC DA DG

SEQRES 8 J 347 DC DT DG DG DA DA DT DC DC DA DG DC DT

SEQRES 9 J 347 DG DA DA DC DA DT DG DC DC DT DT DT DT

SEQRES 10 J 347 DG DA DT DG DG DA DG DC DA DG DT DT DT
SEQRES 11 J 347 DC DC DA DA DA DT DA DC DA DC DT DT DT
SEQRES 12 J 347 DT DG DG DT DA DG DT DA DT DC DT DG DC
SEQRES 13 J 347 DA DG DG DT DT DA DC DA DT DC DC DT DG
SEQRES 14 J 347 DT DG DC DA DT DG DT DA DA DG DT DA DC
SEQRES 15 J 347 DT DG DG DC DC DG DC DC DC DT DG DG DA
SEQRES 16 J 347 DG DA DA DT DC DA DC DC DT DG DC DA DG
SEQRES 17 J 347 DA DT DA DC DT DA DC DC DA DA DA DA DG
SEQRES 18 J 347 DT DG DT DA DT DT DT DG DG DA DA DA DC
SEQRES 19 J 347 DT DG DC DT DC DC DA DT DC DA DA DA DA
SEQRES 20 J 347 DG DG DC DA DT DG DT DT DC DA DG DC DT
SEQRES 21 J 347 DG DG DA DA DT DC DC DA DG DC DT DG DA
SEQRES 22 J 347 DA DC DA DT DG DC DC DT DT DT DT DG DA
SEQRES 23 J 347 DT DG DG DA DG DC DA DG DT DT DT DC DC
SEQRES 24 J 347 DA DA DA DT DA DC DA DC DT DT DT DT DG
SEQRES 25 J 347 DG DT DA DG DT DA DT DC DT DG DC DA DG
SEQRES 26 J 347 DG DT DT DA DC DA DT DC DC DT DG DT DG
SEQRES 27 J 347 DC DA DT DG DT DA DA DG DT

Table S1 The sequence of nucleotides in $DNA_{1/2}$ in the model of the two NCPs is shown in the following SEQRES comment in PDB 1ZBB (18);
DNA_1 (167 nucleotides of I-chain from sequence 1 to 167, shown in green)
DNA_2 (167 nucleotides of I-chain from sequence 168 to 334, shown in brown)
DNA_2 (167 nucleotides of J-chain from sequence 14 to 180, shown in blue)
DNA_1 (167 nucleotides of J-chain from sequence 181 to 347, shown in red)
(Nucleotides of I-chain from sequence 335 to 347 and nucleotides of J-chain from sequence 1 to 13 were truncated in our system.) The nucleotides of $(Cyt22)_1$, $(Thy62)_1$, $(Cyt189)_2$ and $(Thy229)_2$ which are shown in Fig. 1 are marked in bold.

	α-helix	3_{10}-helix	β-strand	turn	bridge	coil
LEFT 1	0.006 (0.040)	0.107 (0.274)	0.007 (0.036)	5.931 (1.835)	0.042 (0.096)	19.907 (1.912)
	0.002 (0.014)	0.039 (0.160)	0.000 (0.000)	7.038 (2.317)	0.025 (0.119)	18.895 (2.324)
	0.000 (0.000)	0.043 (0.199)	0.004 (0.019)	3.041 (0.019)	0.014 (0.044)	13.899 (1.633)
	0.001 (0.006)	0.013 (0.063)	0.005 (0.034)	7.968 (1.244)	0.051 (0.144)	8.963 (1.280)
LEFT 2	0.074 (0.244)	0.180 (0.433)	0.001 (0.005)	7.552 (1.914)	0.091 (0.209)	18.103 (1.959)
	0.039(0.206)	0.081 (0.254)	0.002 (0.015)	7.591 (2.589)	0.078 (0.246)	18.208 (2.583)
	0.000 (0.003)	0.321 (0.539)	0.007 (0.032)	4.877 (1.839)	0.064 (0.137)	11.731 (2.194)
	0.000 (0.000)	0.028 (0.103)	0.000 (0.000)	6.626 (1.507)	0.043 (0.122)	10.303 (1.527)
LEFT 3	0.027 (0.101)	0.558 (0.706)	0.032 (0.099)	6.618 (2.165)	0.362 (0.493)	18.404 (2.199)
	0.022 (0.113)	0.192 (0.113)	0.071 (0.292)	6.367 (2.089)	0.413 (0.448)	18.931 (2.373)
	0.000 (0.000)	0.170 (0.442)	0.011 (0.036)	6.530 (1.499)	0.151 (0.279)	10.137 (1.624)
	0.003 (0.020)	0.114 (0.319)	0.004 (0.029)	5.258 (2.042)	0.100 (0.293)	11.521 (2.265)
RIGHT 1	0.001 (0.009)	0.188 (0.427)	0.465 (0.970)	7.063 (2.657)	0.615 (0.549)	17.668 (2.570)
	0.008 (0.039)	0.631 (0.768)	0.158 (0.630)	8.404 (2.119)	0.302 (0.360)	16.497 (2.298)
	0.000 (0.000)	0.001 (0.009)	0.000 (0.000)	1.122 (1.248)	0.007 (0.056)	15.870 (1.264)
	0.016 (0.130)	0.084 (0.213)	0.003 (0.013)	5.913 (1.604)	0.049 (0.114)	10.935 (1.674)
RIGHT 2	0.001 (0.005)	0.162 (0.414)	0.185 (0.453)	6.723 (2.207)	0.485 (0.475)	18.445 (2.389)
	0.001 (0.007)	0.269 (0.279)	0.007 (0.033)	7.280 (2.021)	0.263 (0.379)	18.178 (2.113)
	0.000 (0.000)	0.070 (0.183)	0.000 (0.000)	4.480 (1.530)	0.018 (0.116)	12.431 (1.618)
	0.022 (0.168)	0.119 (0.344)	0.011 (0.052)	3.013 (1.630)	0.073 (0.262)	13.762 (1.846)
RIGHT 3	0.009 (0.037)	0.093 (0.192)	0.000 (0.000)	4.007 (2.521)	0.019 (0.084)	21.872 (2.647)
	0.004 (0.029)	0.140 (0.412)	1.895 (2.449)	6.850 (2.140)	0.283 (0.370)	16.827 (3.752)
	0.000 (0.000)	0.069 (0.179)	0.057 (0.176)	4.062 (1.345)	0.401 (0.406)	12.410 (1.337)
	0.000 (0.000)	0.248 (0.575)	0.005 (0.020)	6.476 (1.310)	0.105 (0.203)	10.166 (1.481)
PARALLEL 1	0.023 (0.120)	0.237 (0.439)	0.001(0.006)	4.917 (1.918)	0.091 (0.163)	20.731 (2.051)
	0.055 (0.130)	0.049 (0.130)	0.066 (0.187)	6.396 (2.273)	0.297 (0.443)	19.137 (2.504)
	0.000 (0.000)	0.134(0.234)	0.032 (0.078)	5.079 (0.715)	0.293 (0.173)	11.462 (0.699)
	0.041 (0.090)	0.115 (0.146)	0.006 (0.018)	4.422 (0.883)	0.095 (0.126)	12.321 (0.971)
PARALLEL 2	0.000 (0.000)	0.027 (0.072)	0.015 (0.037)	4.213 (1.559)	0.124 (0.236)	21.620 (1.696)
	0.000 (0.000)	0.437 (0.567)	0.002 (0.008)	7.945 (2.499)	0.244 (0.340)	17.373 (2.869)
	0.000 (0.000)	0.040 (0.117)	0.000 (0.000)	2.797 (2.045)	0.016 (0.047)	14.147 (2.085)
	0.000 (0.000)	0.000 (0.000)	0.002 (0.008)	4.443 (1.311)	0.545 (0.509)	12.011 (1.621)

Table S2 The average of a series of average numbers of residues forming secondary structures (α-helix, 3_{10}-helix, β-strand, turn, bridge and coil) along *d* in the 26-residue of the H4 tails 1 and 2 are shown in the first row (in red) and in the second row (in black), respectively. The value in brackets is the root-mean-square-deviation of a series of average numbers of the secondary structures.

	5ns	10ns	15ns	20ns	25ns	30ns
LEFT 1	0.854 (0.074)	0.911 (0.077)	0.943 (0.079)	0.974 (0.020)	0.990 (0.008)	1.000 (0.000)
	0.846 (0.069)	0.909 (0.071)	0.940 (0.073)	0.973 (0.018)	0.989 (0.007)	1.000 (0.000)
	0.873 (0.040)	0.925 (0.040)	0.950 (0.040)	0.978 (0.014)	0.991 (0.007)	1.000 (0.000)
	0.886 (0.034)	0.935 (0.030)	0.960 (0.026)	0.980 (0.016)	0.993 (0.007)	1.000 (0.000)
LEFT 2	0.875 (0.026)	0.931 (0.024)	0.961 (0.018)	0.980 (0.010)	0.992 (0.005)	1.000 (0.000)
	0.856 (0.032)	0.913 (0.025)	0.952 (0.015)	0.976 (0.008)	0.991 (0.004)	1.000 (0.000)
	0.885 (0.036)	0.936 (0.025)	0.964 (0.020)	0.982 (0.015)	0.993 (0.007)	1.000 (0.000)
	0.890 (0.034)	0.942 (0.025)	0.967 (0.017)	0.984 (0.009)	0.994 (0.005)	1.000 (0.000)
LEFT 3	0.864 (0.025)	0.927 (0.021)	0.957 (0.017)	0.976 (0.012)	0.990 (0.006)	1.000 (0.000)
	0.853 (0.031)	0.916 (0.024)	0.950 (0.018)	0.972 (0.013)	0.989 (0.007)	1.000 (0.000)
	0.892 (0.035)	0.942 (0.025)	0.964 (0.016)	0.982 (0.011)	0.993 (0.006)	1.000 (0.000)
	0.891 (0.029)	0.938 (0.023)	0.965 (0.015)	0.981 (0.011)	0.992 (0.006)	1.000 (0.000)
RIGHT 1	0.862 (0.028)	0.921 (0.025)	0.954 (0.019)	0.974 (0.014)	0.989 (0.008)	1.000 (0.000)
	0.860 (0.028)	0.921 (0.021)	0.953 (0.015)	0.976 (0.010)	0.991 (0.005)	1.000 (0.000)
	0.890 (0.027)	0.928 (0.021)	0.954 (0.016)	0.979 (0.014)	0.989 (0.007)	1.000 (0.000)
	0.872 (0.033)	0.927 (0.031)	0.957 (0.023)	0.976 (0.014)	0.992 (0.007)	1.000 (0.000)
RIGHT 2	0.855 (0.032)	0.920 (0.021)	0.953 (0.013)	0.974 (0.011)	0.990 (0.006)	1.000 (0.000)
	0.854 (0.029)	0.919 (0.020)	0.952 (0.016)	0.974 (0.011)	0.990 (0.006)	1.000 (0.000)
	0.894 (0.028)	0.943 (0.021)	0.969 (0.015)	0.983 (0.012)	0.993 (0.007)	1.000 (0.000)
	0.881 (0.035)	0.935 (0.022)	0.965 (0.015)	0.982 (0.010)	0.993 (0.006)	1.000 (0.000)
RIGHT 3	0.857 (0.027)	0.915 (0.023)	0.946 (0.021)	0.971 (0.012)	0.989 (0.006)	1.000 (0.000)
	0.852 (0.035)	0.912 (0.030)	0.942 (0.027)	0.968 (0.014)	0.988 (0.008)	1.000 (0.000)
	0.881 (0.034)	0.927 (0.036)	0.950 (0.036)	0.977 (0.014)	0.992 (0.006)	1.000 (0.000)
	0.890 (0.038)	0.940 (0.025)	0.965 (0.021)	0.983 (0.014)	0.993 (0.008)	1.000 (0.000)
PARALLEL 1	0.863 (0.020)	0.921 (0.017)	0.953 (0.012)	0.973 (0.008)	0.989 (0.004)	1.000 (0.000)
	0.855 (0.030)	0.917 (0.024)	0.950 (0.016)	0.972 (0.012)	0.989 (0.007)	1.000 (0.000)
	0.888 (0.028)	0.936 (0.026)	0.965 (0.016)	0.980 (0.011)	0.992 (0.008)	1.000 (0.000)
	0.881 (0.033)	0.931 (0.026)	0.958 (0.022)	0.974 (0.017)	0.988 (0.011)	1.000 (0.000)
PARALLEL 2	0.870 (0.032)	0.922 (0.028)	0.954 (0.021)	0.974 (0.017)	0.989 (0.008)	1.000 (0.000)
	0.851 (0.035)	0.906 (0.028)	0.945 (0.024)	0.972 (0.014)	0.987 (0.009)	1.000 (0.000)
	0.904 (0.034)	0.941 (0.025)	0.965 (0.016)	0.983 (0.008)	0.994 (0.005)	1.000 (0.000)
	0.902 (0.039)	0.940 (0.035)	0.963 (0.026)	0.980 (0.019)	0.992 (0.008)	1.000 (0.000)

Table S3 The average ratios of the conformational entropies of the H4 tails$_{1/2}$ and H2A tails$_{1/2}$ for 5 ns (from 10 to 15 ns), 10 ns (from 10 to 20 ns), 15 ns (from 10 to 25 ns), 20 ns (from 10 to 30 ns), 25 ns (from 5 to 30 ns) and 30 ns (from 0 to 30 ns) of the umbrella sampling simulations are listed in the first/second (in red) and third/fourth (in black) rows, respectively. The value in brackets is the root-mean-square-deviation of the ratios.

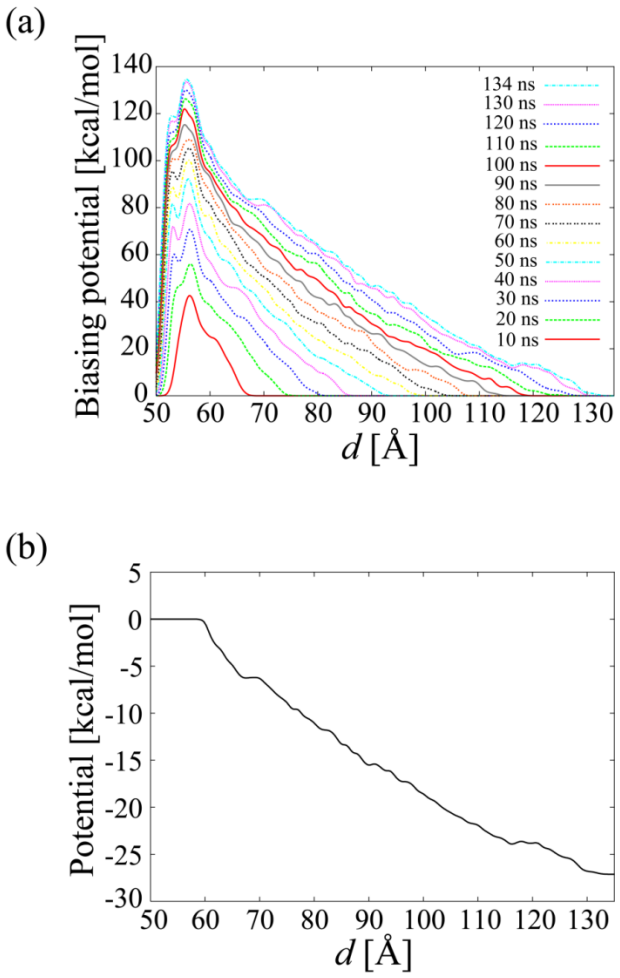

Fig. S1 (a) The evolution of the biasing potential (b) the biasing potential of the second term in Eq. (S3) (or Eq. (3)) used for the umbrella sampling simulations

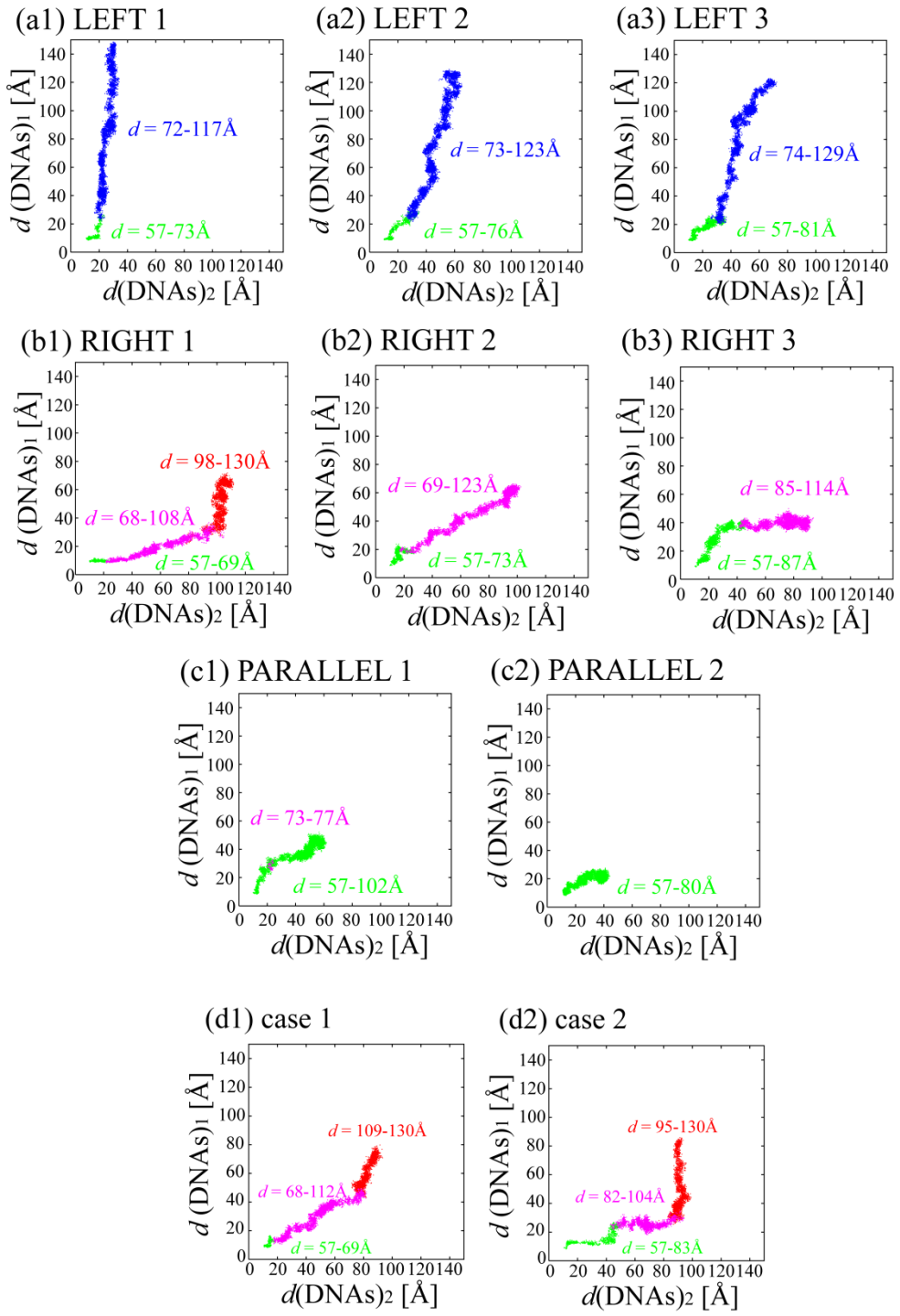

Fig. S2 The trajectories of $d(\mathrm{DNAs})_{2/1}$ of the eight selected models: (a) LEFTs 1-3, (b) RIGHTs 1-3, (c) PARALLELs 1-2 and (d) cases 1-2 which had the breakages of both of the $\mathrm{H4}_{2/1}$ tails, respectively The coloring is the same as that in Fig. 2. The ranges of *d* for each H4 tail-bridge formation are shown in the same color.

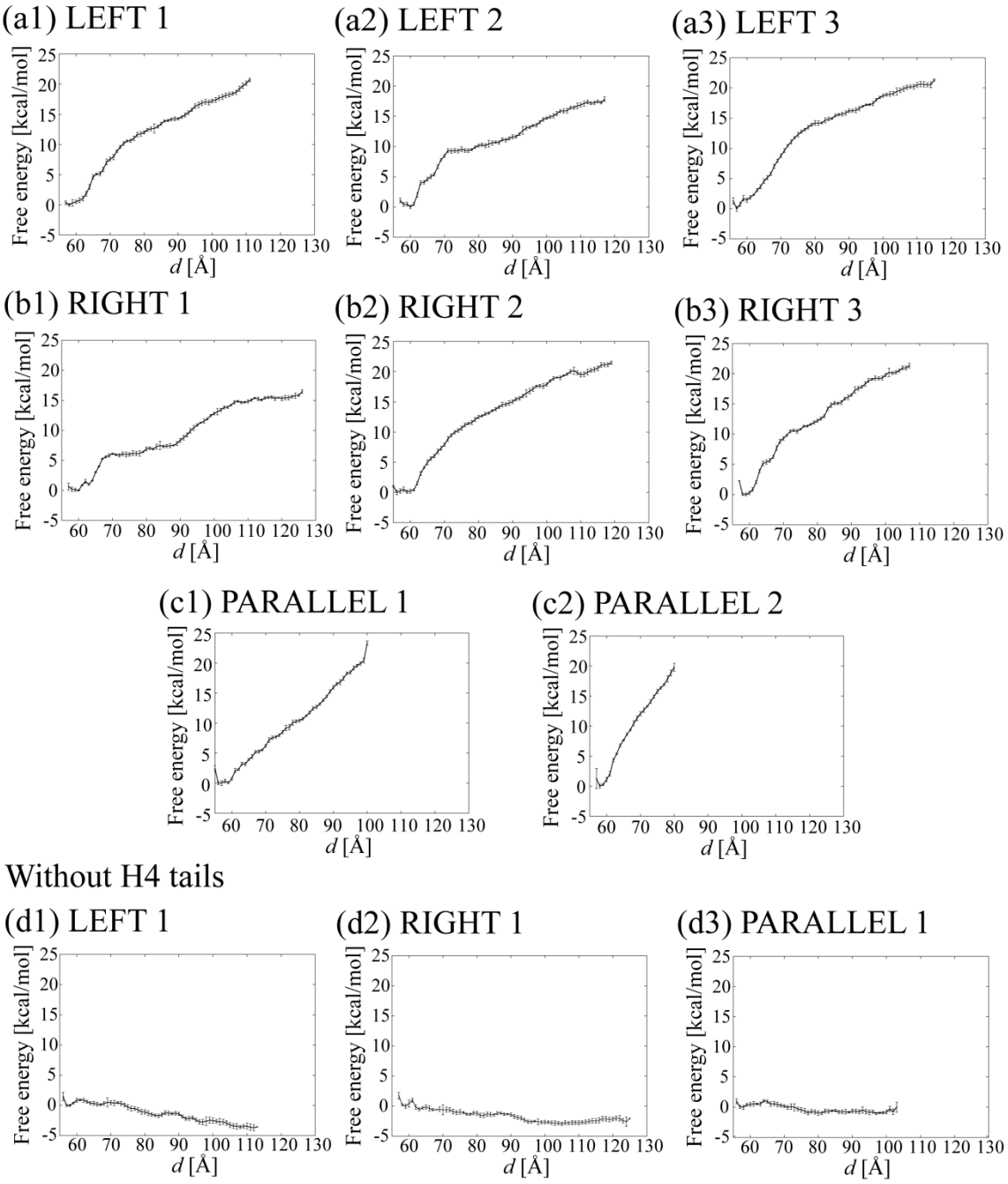

Fig. S3 Errors in the free-energies in (a) LEFTs 1-3, (b) RIGHTs 1-3, (c) PARALLELEs 1-2 and (d) RIGHT 1, LEFT 1 and PARALLEL 1 without the H4 tails. The root mean square errors (RMSEs) in the free-energies were determined by calculating free-energies for four non-overlapping segments (from 0 to 5 ns, from 5 to 10ns, 10 to 15 ns, and 15 to 20) of the 20 ns trajectory of the umbrella sampling simulations. Each free-energy which was calculated from a 5 ns trajectory was aligned to the final free-energy which was calculated from the 20 ns trajectory so that the

average of the free-energy coincides with the average of the final free-energy. To calculate the average of the free-energy, the values of the free-energy at *d* which were estimated using sufficient sampling data (more than 1% of the number of data points (20,000) for each segment in the window) were used; as for the NCPs with the H4 tails, in the range of *d* = 57 to 110 Å in LEFT 1, 57 to 117 Å in LEFT 2, and 57 to 114 Å in LEFT 3, 57 to 126 Å in RIGHT1, 56 to 119 Å in RIGHT2, 58 to 107 Å in RIGHT3, 56 to 99 Å in PARALLEL 1 and 58 to 80 Å in PARALLEL2. As for the NCPs without the H4 tails, in the range of *d* = 57 to 112 Å in LEFT 1, 57 to 124 Å in RIGHT 1, and 56 to 102 Å in PARALELL 1.

The RMSE for each system was calculated using the equation, $\sqrt{\sum_{k=1}^{n}\left(f_k(d)-\bar{f}\right)^2/(n-1)}$, where $f_k(d)$ is the value of the aligned free-energy at *d* and $\bar{f}$ is the average and *n* is the number of segments at *d* for each system (n is usually 4 except at *d* where sampling data is scarce). The RMSEs are shown in error bars along the final free-energy. The averages of the errors in the free-energies of the NCPs with H4 tails along *d* (within the range of sufficient sampling data) were 0.33, 0.30 and 0.31 kcal/mol in LEFTs 1-3, 0.25, 0.30 and 0.28 kcal/mol RIGHTs 1-3, 0.26 and 0.30 kcal/mol in PARALLELs 1-2, respectively. The errors in the free-energies of the NCPs without H4 tails were 0.34, 0.31 and 0.32 kcal/mol in LEFT 1, RIGHT 1, and PARALELL 1, respectively. The units of the free-energy and error are kcal/mol.

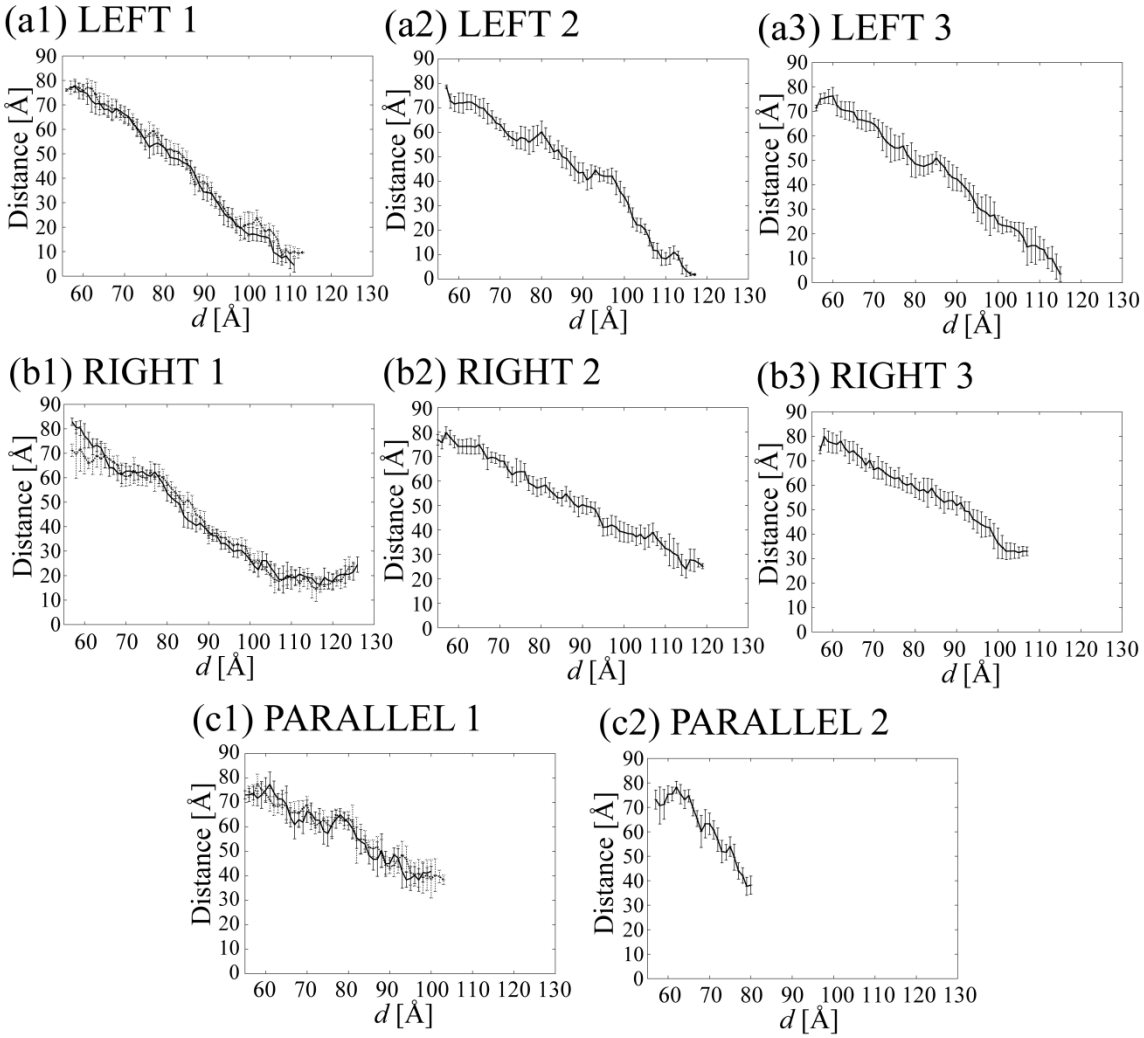

Fig. S4 The distance in the *z*-direction between NCP_1 in the system and NCP_2 in the mirror image in (a) LEFTs 1-3, (b) RIGHTs 1-3 and (c) PARALLELs 1-2. Each distance in LEFTs 1-3, RIGHTs 1-3 and PARALLELs 1-2 with the H4 tails is shown by a solid line, and each distance in LEFT 1, RIGHT 1 and PARALLEL 1 without the H4 tails is shown by a dotted line. The unit is Å.

(a1) LEFT 1

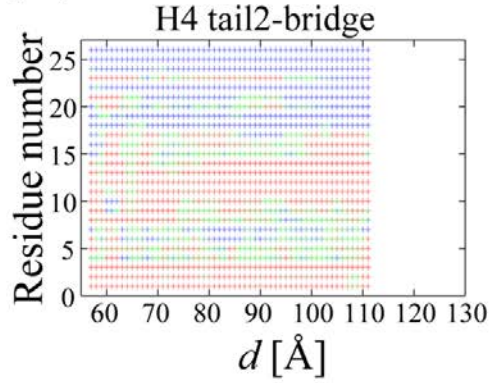

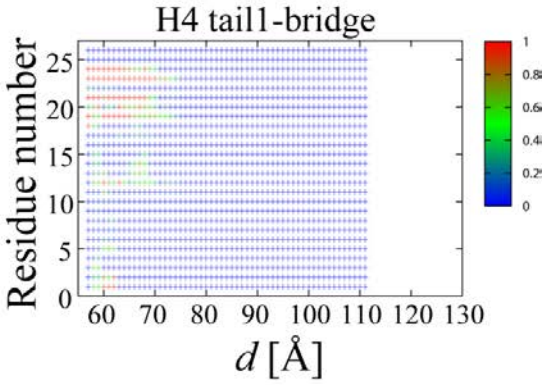

(a2) LEFT 2

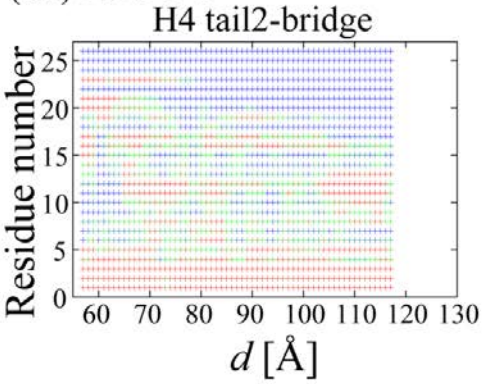

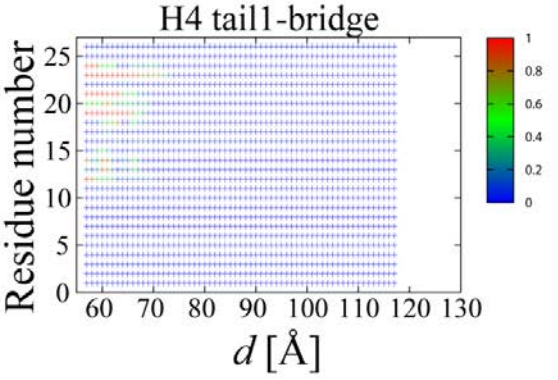

(a3) LEFT 3

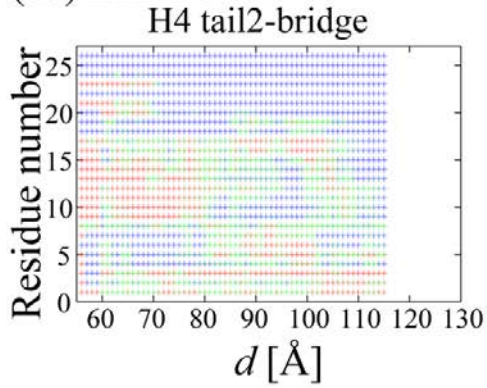

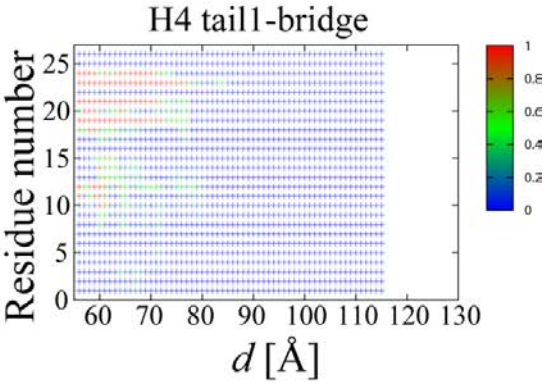

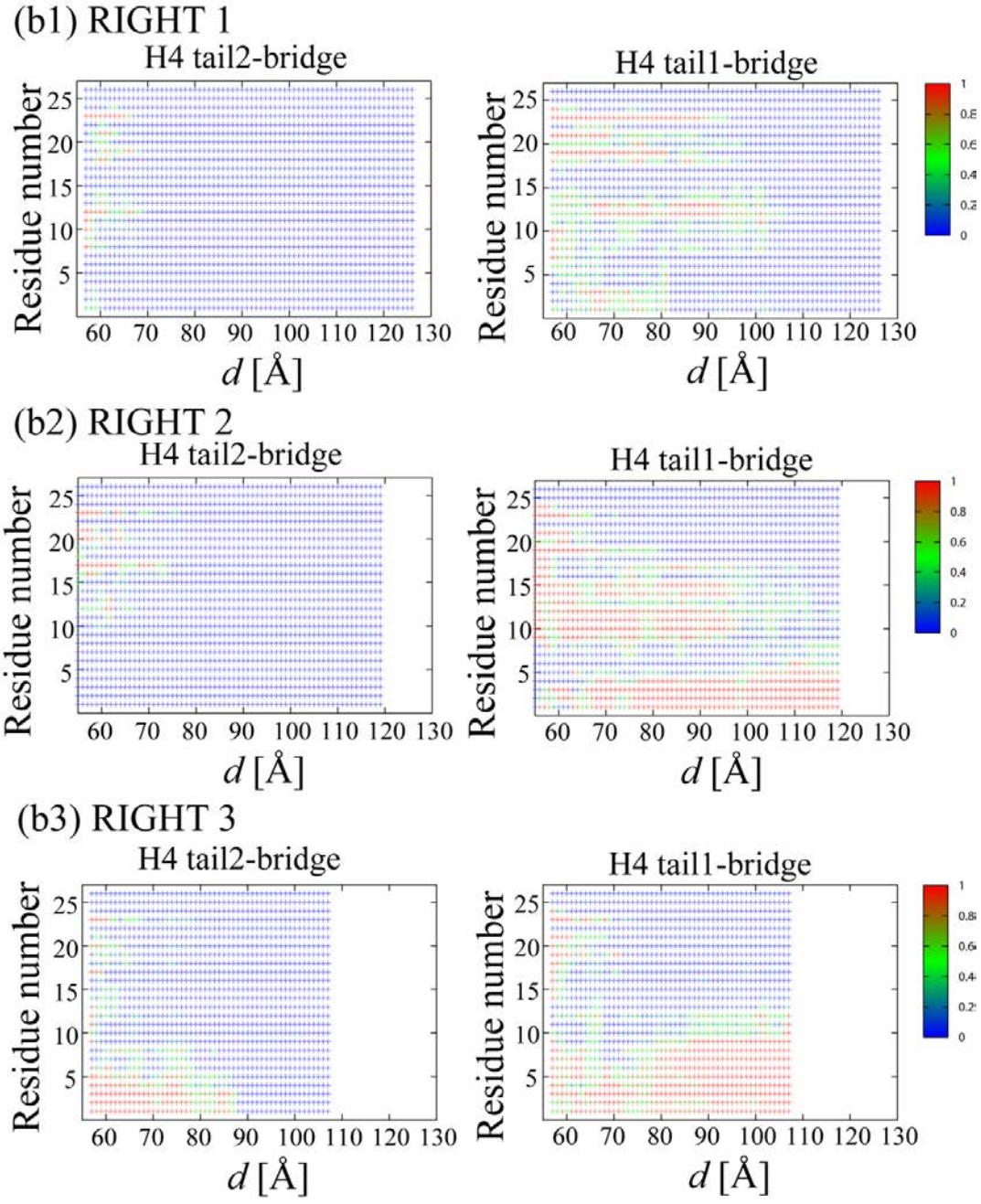
(b1) RIGHT 1
H4 tail2-bridge
H4 tail1-bridge
Residue number
d [Å]
(b2) RIGHT 2
H4 tail2-bridge
H4 tail1-bridge
Residue number
d [Å]
(b3) RIGHT 3
H4 tail2-bridge
H4 tail1-bridge
Residue number
d [Å]

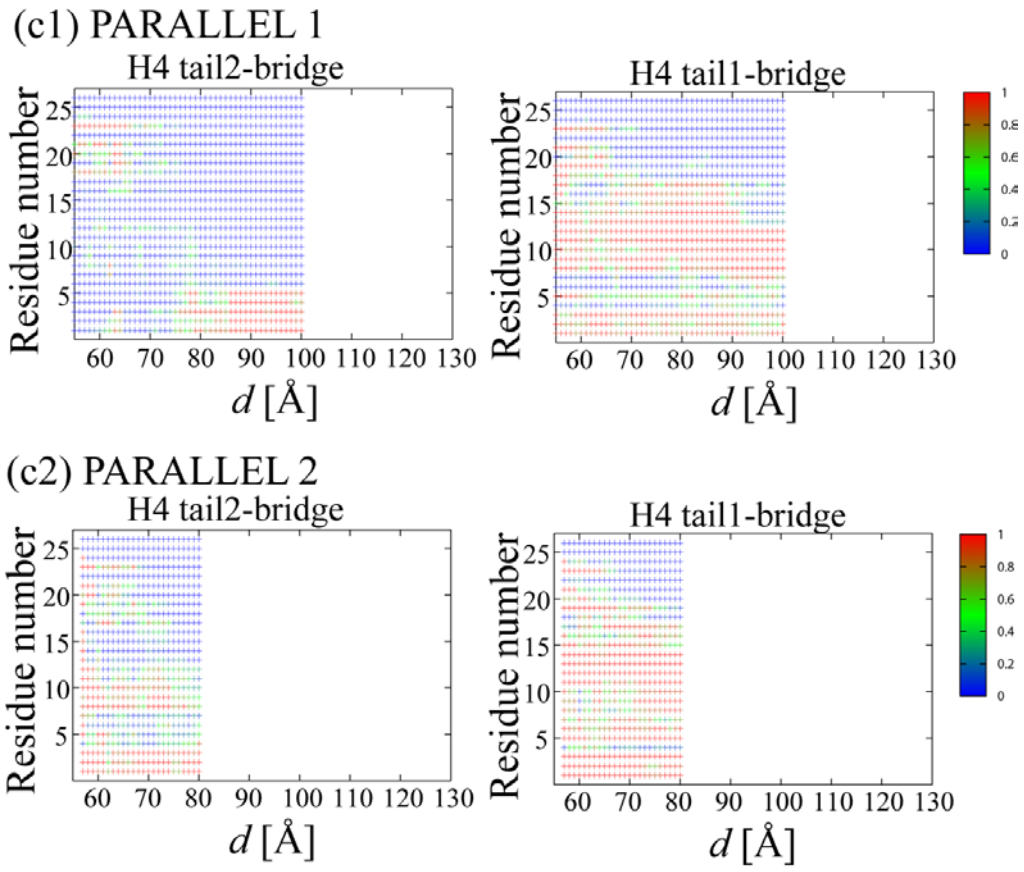

Fig. S5 The average population of residues which participated in the formation of H4 $tail_{1/2}$-bridge in (a) LEFTs 1-3, (b) RIGHTs 1-3 and (c) PARALLELs 1-2. The average was calculated according to Eq. (S8).

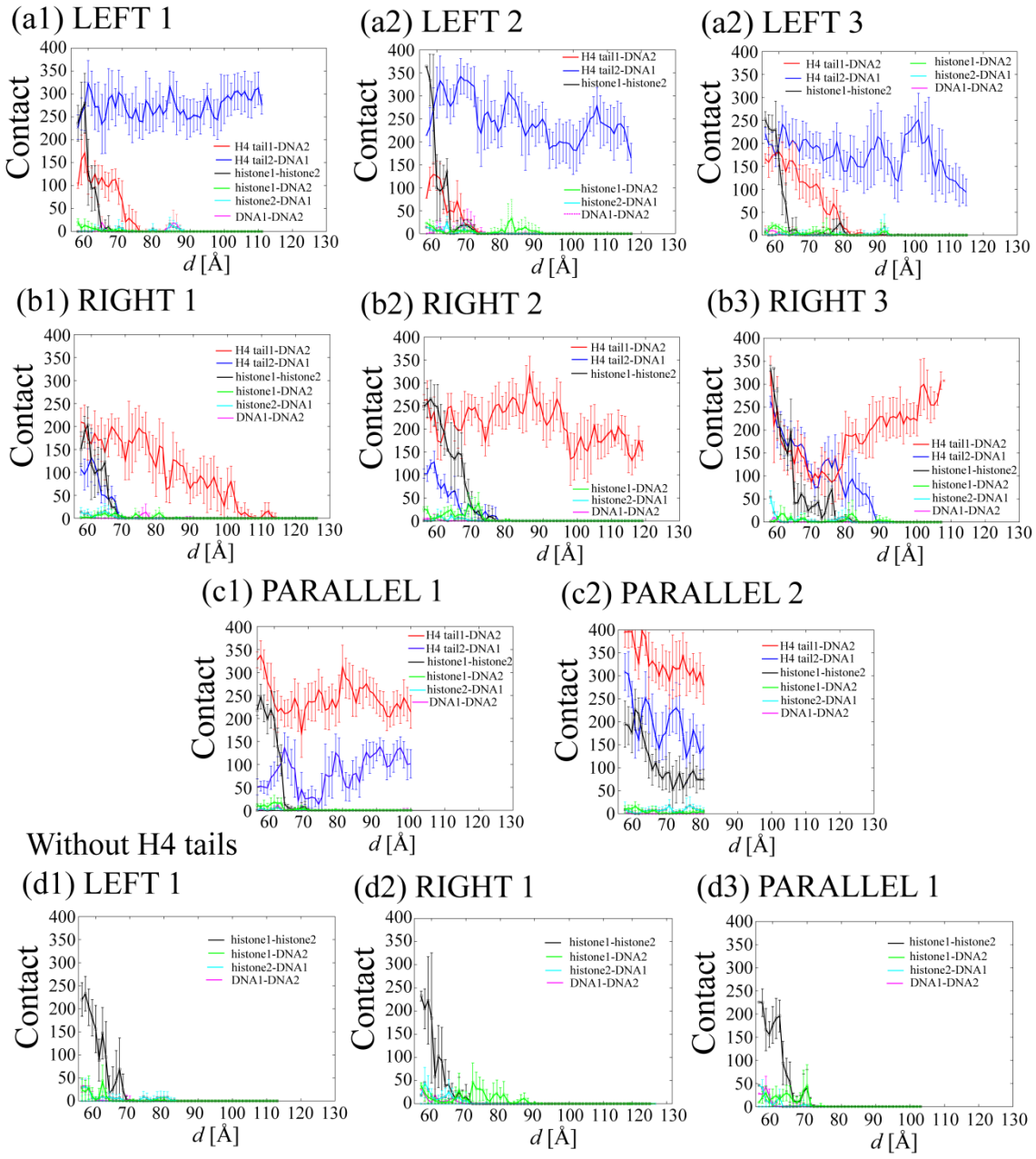

Fig. S6 The number of contacts between the NCPs (H4 $tail_{1/2}$ – $DNA_{2/1}$, $histone_1$ – $histone_2$ (excluding the H4 tails), $histone_{1/2}$ – $DNA_{2/1}$ and DNA_1 – DNA_2) in (a) LEFTs 1-3, (b) RIGHTs 1-3, (c) PARALLELs 1-2 and (d) RIGHT 1, LEFT 1 and PARALLEL 1 without the H4 tails. The contacts between H4 $tail_{1/2}$ and $histone_{2/1}$ were not observed in this study.

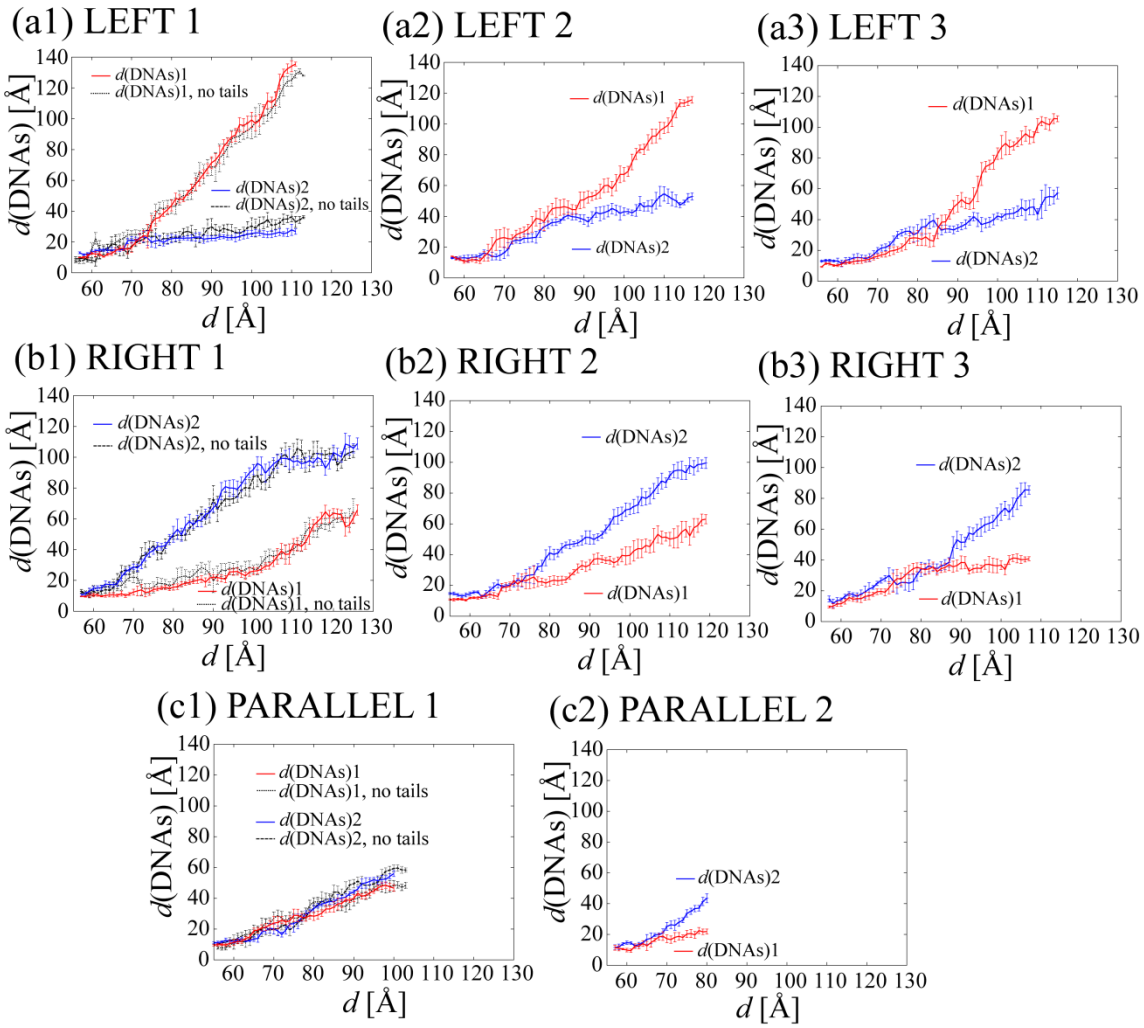

Fig. S7 $d(\mathrm{DNAs})_{2/1}$ against d for (a) LEFTs 1-3, (b) RIGHTs 1-3and (c) PARALLELs 1-2. The average and RMSD were calculated according to Eqs. (S8) and (S9), respectively.

(a1) LEFT 1

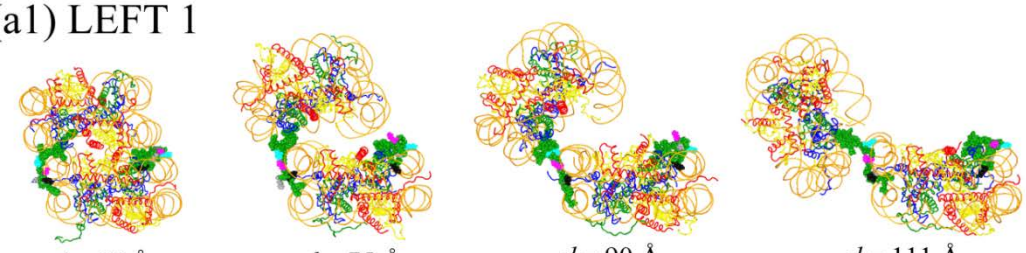

d = 58 Å (12.5 / 10.8 Å)

d = 75 Å (19.5 / 32.0 Å)

d = 90 Å (22.4 / 71.5 Å)

d = 111 Å (26.4 / 136.6 Å)

(a2) LEFT 1 (without H4 tails)

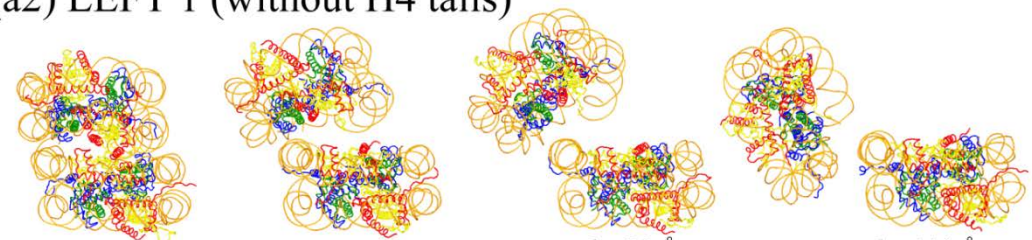

d = 58 Å (9.5 / 7.3 Å)

d = 75 Å (23.0 / 31.6 Å)

d = 90 Å (28.8 / 68.5 Å)

d = 111 Å (34.0 / 129.6 Å)

(a3) LEFT 2

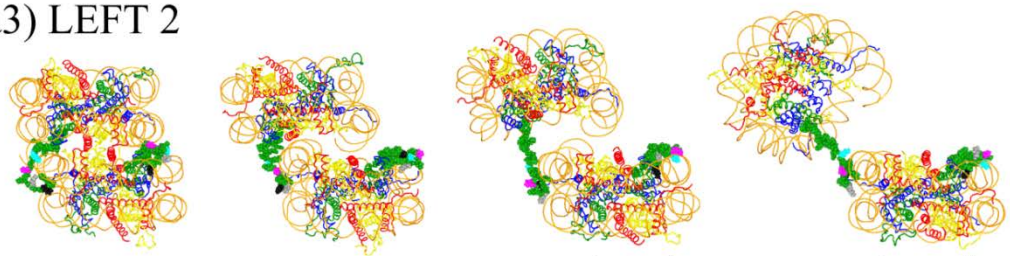

d = 58 Å (13.1 / 12.8 Å)

d = 74 Å (24.8 / 29.4 Å)

d = 90 Å (37.6 / 50.1 Å)

d = 117 Å (52.6 / 116.1 Å)

(a4) LEFT 3

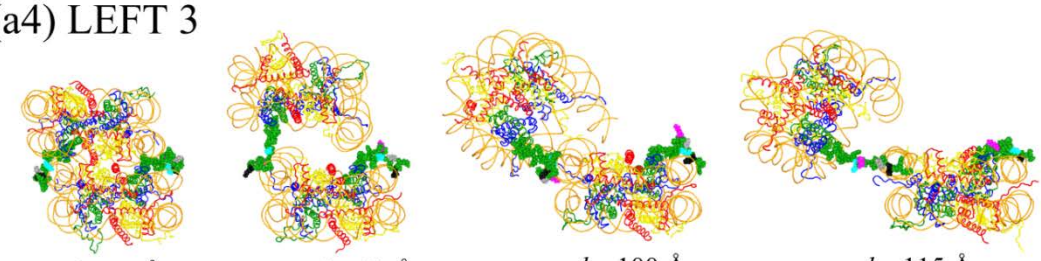

d = 58 Å (13.6 / 11.0 Å)

d = 81 Å (34.1 / 26.7 Å)

d = 100 Å (42.6 / 82.7 Å)

d = 115 Å (57.8 / 105.7 Å)

(b1) RIGHT 1

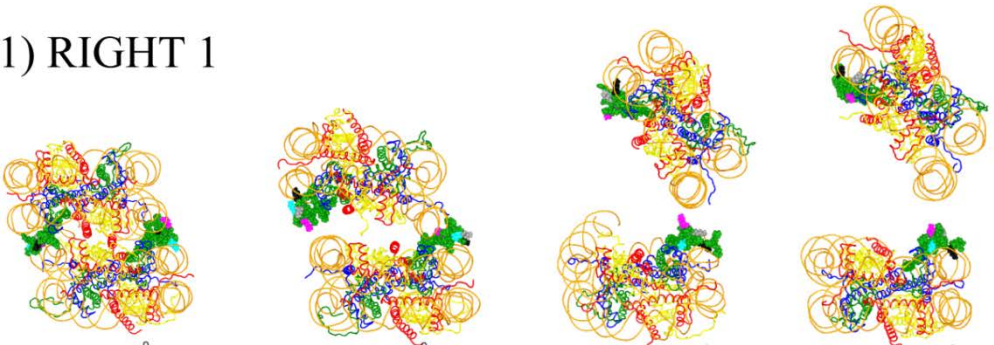

d = 58 Å (11.5 / 9.6 Å)

d = 70 Å (28.5 / 12.1 Å)

d = 108 Å (99. 2 / 35.3 Å)

d = 125 Å (105.2 / 60.5 Å)

(b2) RIGHT 1 (without H4 tails)

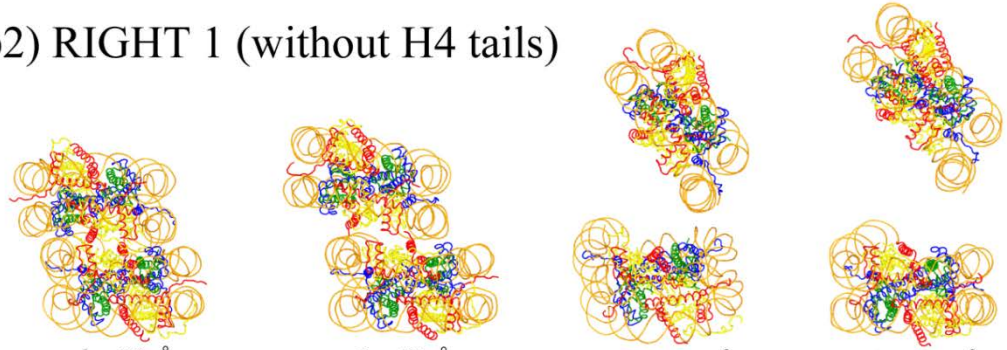

d = 58 Å (11.1 / 11.1 Å)

d = 70 Å (28.7 / 22.2 Å)

d = 108 Å (102.6 / 38.7 Å)

d = 125 Å (104.0 / 65.8 Å)

(b3) RIGHT 2

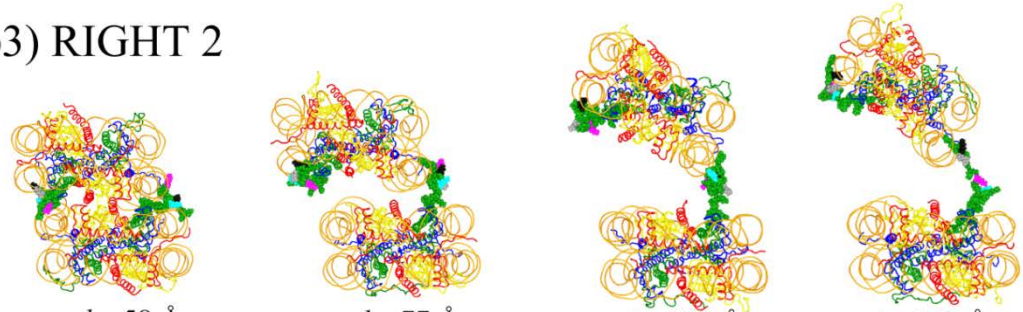

d = 58 Å (13.3 / 10.8 Å)

d = 77 Å (31.4 / 22.9 Å)

d = 100 Å (69.3 / 38.4 Å)

d = 119 Å (99.0 / 63.4 Å)

(b4) RIGHT 3

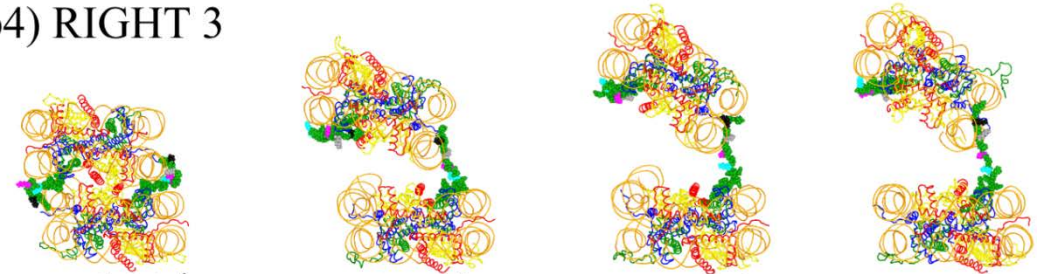

d = 58 Å (11.7 / 10.2 Å)

d = 89 Å (52.0 / 36.6 Å)

d = 100 Å (71.1 / 35.8 Å)

d = 107 Å (85.6 / 40.3 Å)

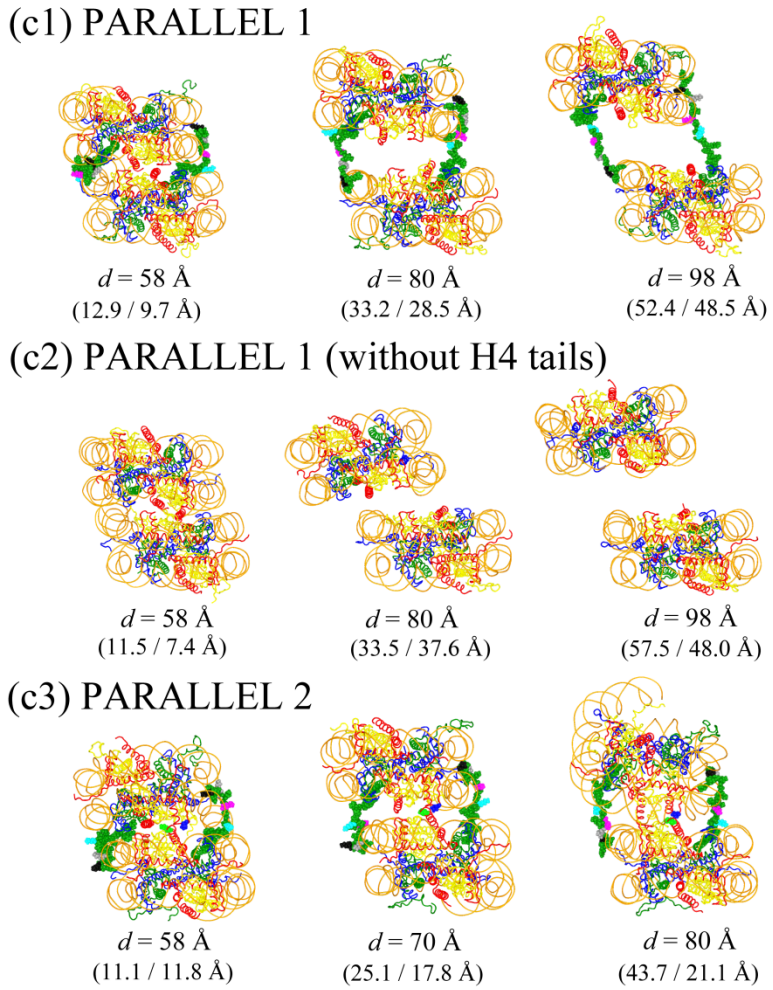

Fig. S8 The snap shots of the NCP-NCP conformations whose $d(\mathrm{DNAs})_{2/1}$ are close to their averages at each d are shown. The value in the bracket after $d(\mathrm{DNAs})_{2/1}$ is the averaged value of $d(\mathrm{DNAs})_{2/1}$ at d. Lys5, Lys8, Lys12 and Lys16 in the H4 $\mathrm{tails}_{2/1}$ are shown in CPK models in black, grey, magenta and cyan, respectively. The side view for each conformation is slightly different from each other for the sake of visual clarity. In PARALLEL 2, Lys177 in $\mathrm{H2B_1}$ and Pro47 in $\mathrm{H2B_2}$ are shown in CPK models in thin green and blue, respectively. It should be noted that $d(\mathrm{DNAs})_{2/1}$ are not necessarily discernable in this figure; for example, although $d(\mathrm{DNAs})_2$ in PARALLEL 1 without the H4 tails, 57.5Å is larger than that with the H4 tails, 52.4Å, the former looks shorter because the $\mathrm{NCP_2}$ has been slid forward and this movement cannot be shown in this figure.

The value of $d(\mathrm{DNAs})_{2/1}$ in the figure and average value of $d(\mathrm{DNAs})_{2/1}$ at each d are shown as follows (the average value is shown in brackets):

(a1) LEFT 1 (i) d = 58 Å, $d(\mathrm{DNAs})_{2/1}$ = 12.5 / 10.8 Å (12.4 / 10.5 Å) ii) d = 75 Å,

d(DNAs)$_{2/1}$ = 19.5 / 32.0 Å, (19.8 / 32.1 Å) (iii) d = 90 Å, d(DNAs)$_{2/1}$ = 22.4 / 71.5 Å (22.4 / 71.4 Å) and (iv) d = 111 Å, d(DNAs)$_{2/1}$ = 26.4 / 136.6 Å (135.5 / 26.8 Å)
(a2) LEFT 1 without the H4 tails (i) d = 58 Å, d(DNAs)$_{2/1}$ = 9.5 / 7.3 Å (9.4 / 7.3 Å) ii) d = 75 Å, d(DNAs)$_{2/1}$ = 23.0 / 31.6 Å (23.0 / 31.8 Å), (iii) d = 90 Å, d(DNAs)$_{2/1}$ = 28.8 / 68.5 Å (29.6 / 68.6 Å) and (iv) d = 111 Å, d(DNAs)$_{2/1}$ = 34.0 / 129.6 Å (34.5 / 128.9 Å)
(a3) LEFT 2 (i) d = 58 Å, d(DNAs)$_{2/1}$ = 13.1 / 12.8 Å (13.0 / 12.8 Å) ii) d = 74 Å, d(DNAs)$_{2/1}$ = 24.8 / 29.4 Å (24.3 / 29.1 Å), (iii) d = 90 Å, d(DNAs)$_{2/1}$ = 37.6 / 50.1 Å (37.9 / 50.8 Å) and (iv) d = 117 Å, d(DNAs)$_{2/1}$ = 52.6 / 116.1 Å (52.9 / 115.7 Å)
(a4) LEFT 3 (i) d = 58 Å, d(DNAs)$_{2/1}$ = 13.6 / 11.0 Å (13.5 / 11.3 Å) ii) d = 81 Å, d(DNAs)$_{2/1}$ = 34.1 / 26.7 Å (35.0 / 27.2 Å), (iii) d = 100 Å, d(DNAs)$_{2/1}$ = 42.6 / 82.7 Å (42.3 / 82.8 Å) and (iv) d = 115 Å, d(DNAs)$_{2/1}$ = 57.8 / 105.7 Å (57.2 / 105.5 Å)

(b1) RIGHT 1 (i) d = 58 Å, d(DNAs)$_{2/1}$ = 11.5 / 9.6 Å (11.3 / 9.5 Å) ii) d = 70 Å, d(DNAs)$_{2/1}$ = 28.5 / 12.1 Å (28.7 / 12.4 Å), (iii) d = 108 Å, d(DNAs)$_{2/1}$ = 99.2 / 35.3 Å (99.2 / 36.8 Å) and (iv) d = 125 Å, d(DNAs)$_{2/1}$ = 105.2 / 60.5 Å (105.8 / 60.7 Å)
(b2) RIGHT 1 without the H4 tails (i) d = 58 Å, d(DNAs)$_{2/1}$ = 11.1 / 11.1 Å (11.1 / 11.4 Å) ii) d = 70 Å, d(DNAs)$_{2/1}$ = 28.7 / 22.2 Å (28.5 / 22.1 Å), (iii) d = 108 Å, d(DNAs)$_{2/1}$ = 102.6 / 38.7 Å (101.7 / 38.4 Å) and (iv) d = 125 Å, d(DNAs)$_{2/1}$ = 104.0 / 65.8 Å (103.8 / 65.0 Å)
(b3) RIGHT 2 (i) d = 58 Å, d(DNAs)$_{2/1}$ = 13.3 / 10.8 Å (13.1 / 10.8 Å) ii) d = 77 Å, d(DNAs)$_{2/1}$ = 31.4 / 22.9 Å (32.1 / 22.4 Å), (iii) d = 100 Å, d(DNAs)$_{2/1}$ = 69.3 / 38.4 Å (69.6 / 39.5 Å) and (iv) d = 119 Å, d(DNAs)$_{2/1}$ = 99.0 / 63.4 Å (99.6 / 63.1 Å)
(b4) RIGHT 3 (i) d = 58 Å, d(DNAs)$_{2/1}$ = 11.7 / 10.2 Å (11.7 / 10.0 Å) ii) d = 89 Å, d(DNAs)$_{2/1}$ = 52.0 / 36.6 Å, (52.9 / 36.4 Å) (iii) d = 100 Å, d(DNAs)$_{2/1}$ = 71.1 / 35.8 Å (71.0 / 36.6 Å) and (iv) d = 107 Å, d(DNAs)$_{2/1}$ = 85.61 / 40.3 Å (85.4 / 40.7 Å)

(c1) PARALLEL 1 (i) d = 58 Å, d(DNAs)$_{2/1}$ = 12.9 / 9.7 Å (12.8 / 9.7 Å) ii) d = 80 Å, d(DNAs)$_{2/1}$ = 33.2 / 28.5 Å (33.3 / 28.4 Å) iii) d = 98 Å, d(DNAs)$_{2/1}$ = 52.4 / 48.5 Å (52.4 / 48.5 Å)
(c2) PARALLEL 1 without the H4 tails (i) d = 58 Å, d(DNAs)$_{2/1}$ = 11.5 / 7.4 Å (11.6 / 7.7 Å) ii) d = 80 Å, d(DNAs)$_{2/1}$ = 33.5 / 37.6 (33.5 / 37.6 Å) iii) d = 98 Å, d(DNAs)$_{2/1}$ = 57.5 / 48.0 Å (57.5 / 48.2 Å)
(c3) PARELLEL 2 (i) d = 58 Å, d(DNAs)$_{2/1}$ = 11.1 / 11.8 Å (11.6 / 11.4 Å) ii) d = 70 Å, d(DNAs)$_{2/1}$ = 25.1 / 17.8 Å (25.3 / 17.2 Å) and (iii) d = 80 Å, d(DNAs)$_{2/1}$ = 43.7 / 21.1 Å (43.5 / 21.9 Å)

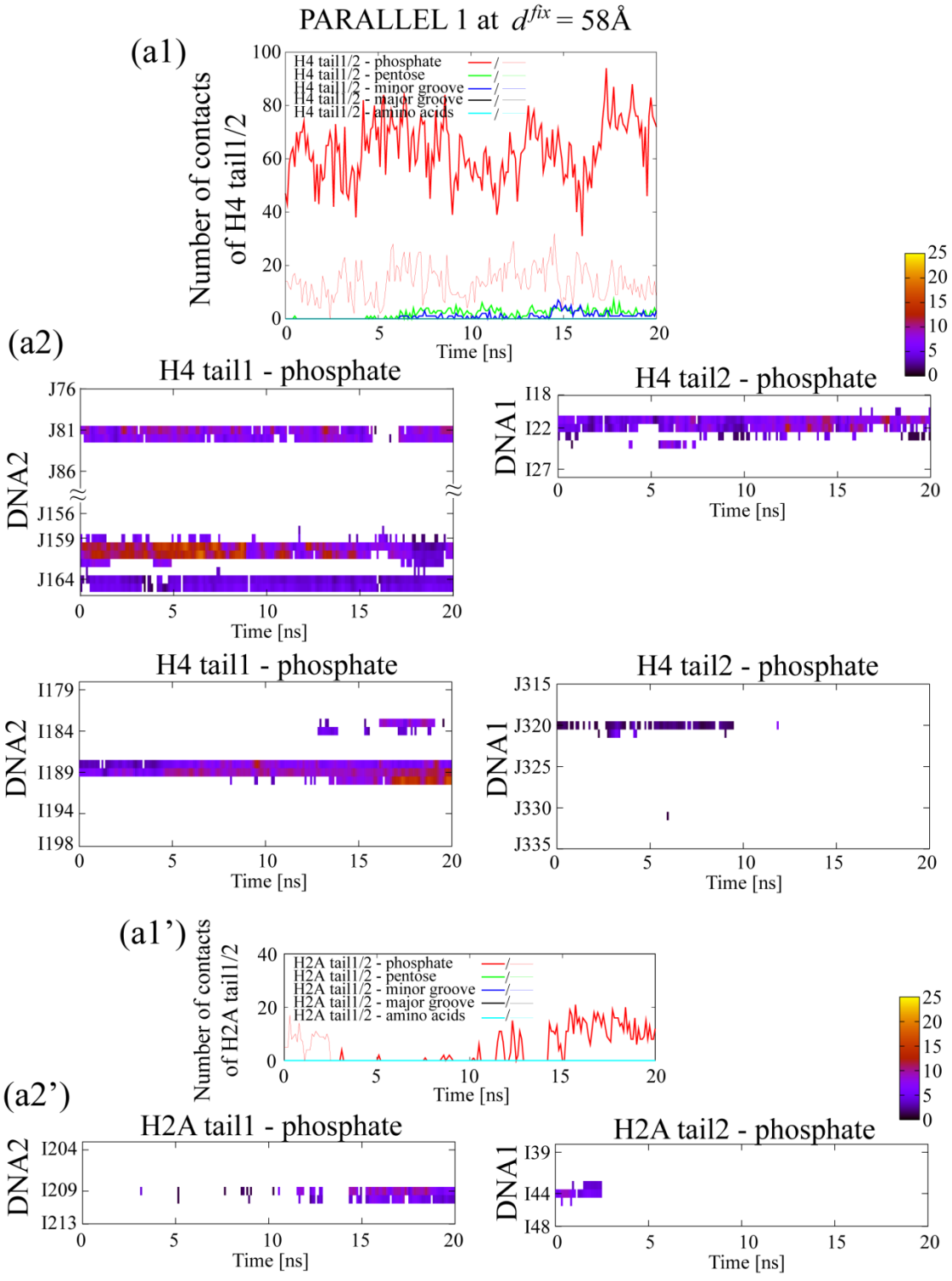
PARALLEL 1 at d^{fix} = 58Å
(a1)
Number of contacts of H4 tail1/2
H4 tail1/2 - phosphate
H4 tail1/2 - pentose
H4 tail1/2 - minor groove
H4 tail1/2 - major groove
H4 tail1/2 - amino acids
Time [ns]
(a2)
H4 tail1 - phosphate
H4 tail2 - phosphate
DNA2
DNA1
Time [ns]
(a1')
Number of contacts of H2A tail1/2
H2A tail1/2 - phosphate
H2A tail1/2 - pentose
H2A tail1/2 - minor groove
H2A tail1/2 - major groove
H2A tail1/2 - amino acids
(a2')
H2A tail1 - phosphate
H2A tail2 - phosphate

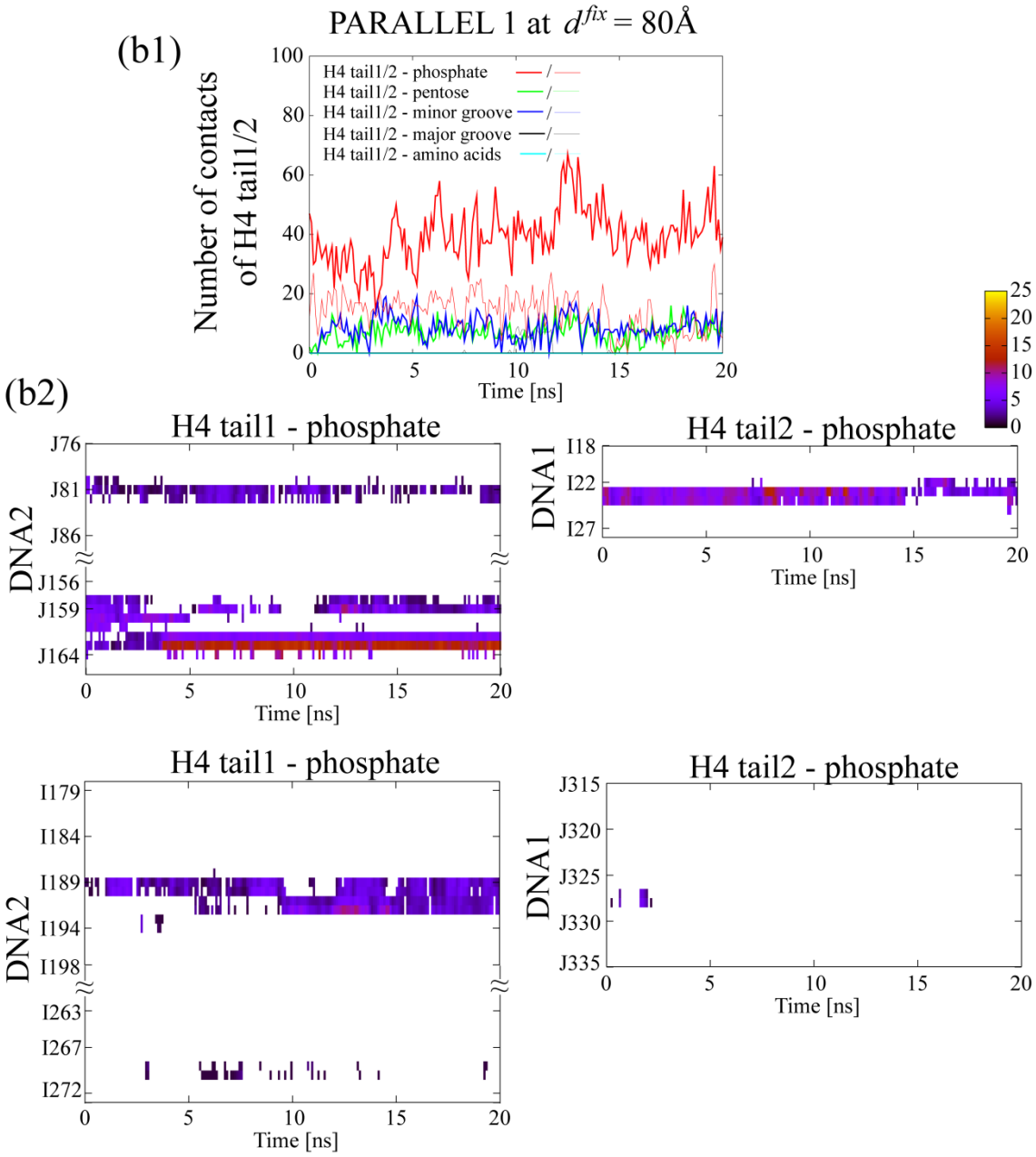
(b1)
PARALLEL 1 at d^{fix} = 80Å
Number of contacts of H4 tail1/2
H4 tail1/2 - phosphate
H4 tail1/2 - pentose
H4 tail1/2 - minor groove
H4 tail1/2 - major groove
H4 tail1/2 - amino acids
Time [ns]
(b2)
H4 tail1 - phosphate
H4 tail2 - phosphate
DNA2
DNA1
Time [ns]

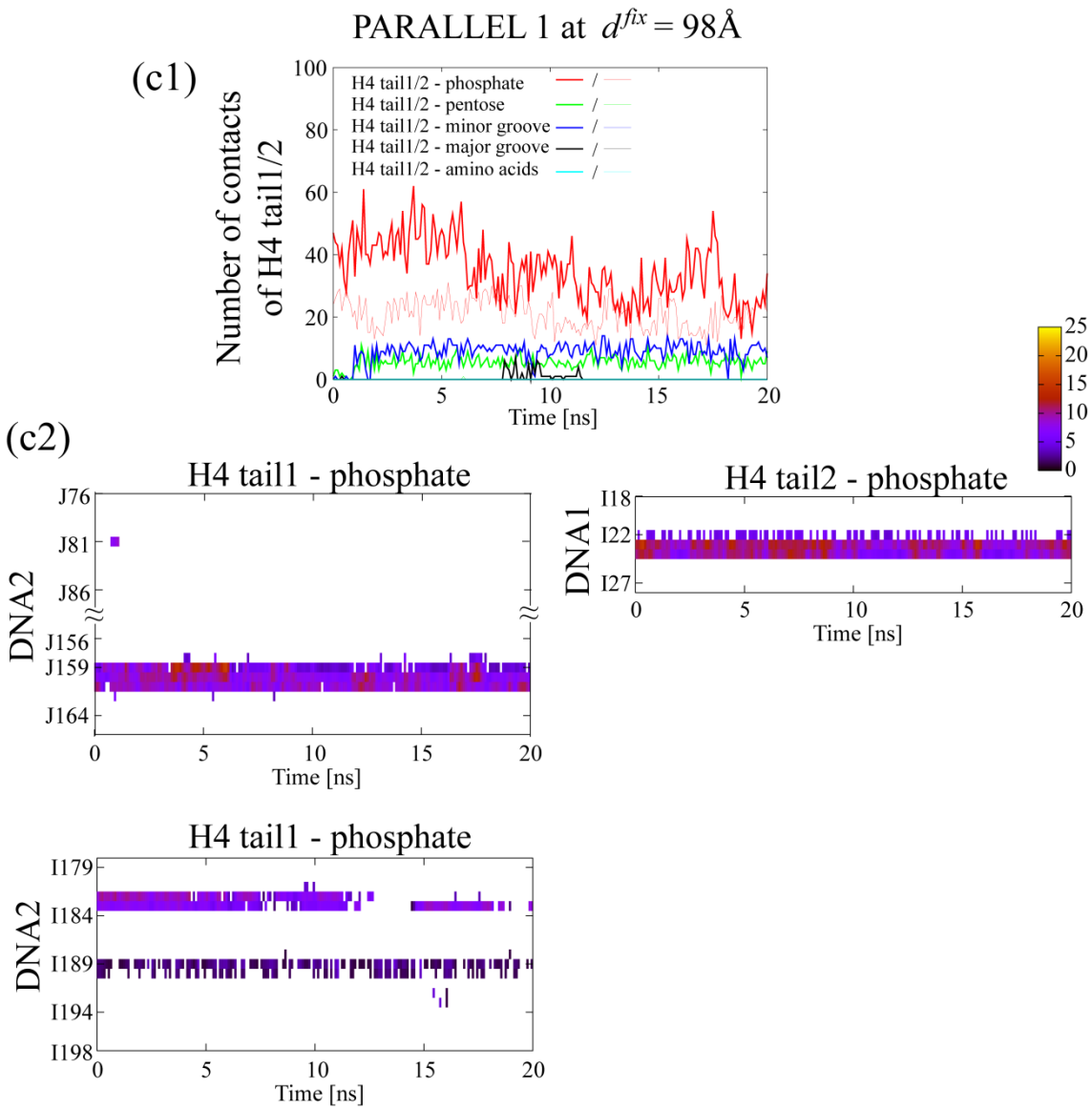
PARALLEL 1 at $d^{fix} = 98$Å
(c1)
Number of contacts of H4 tail1/2
H4 tail1/2 - phosphate
H4 tail1/2 - pentose
H4 tail1/2 - minor groove
H4 tail1/2 - major groove
H4 tail1/2 - amino acids
Time [ns]
(c2)
H4 tail1 - phosphate
DNA2
J76
J81
J86
J156
J159
J164
Time [ns]
H4 tail2 - phosphate
DNA1
I18
I22
I27
Time [ns]
H4 tail1 - phosphate
DNA2
I179
I184
I189
I194
I198
Time [ns]

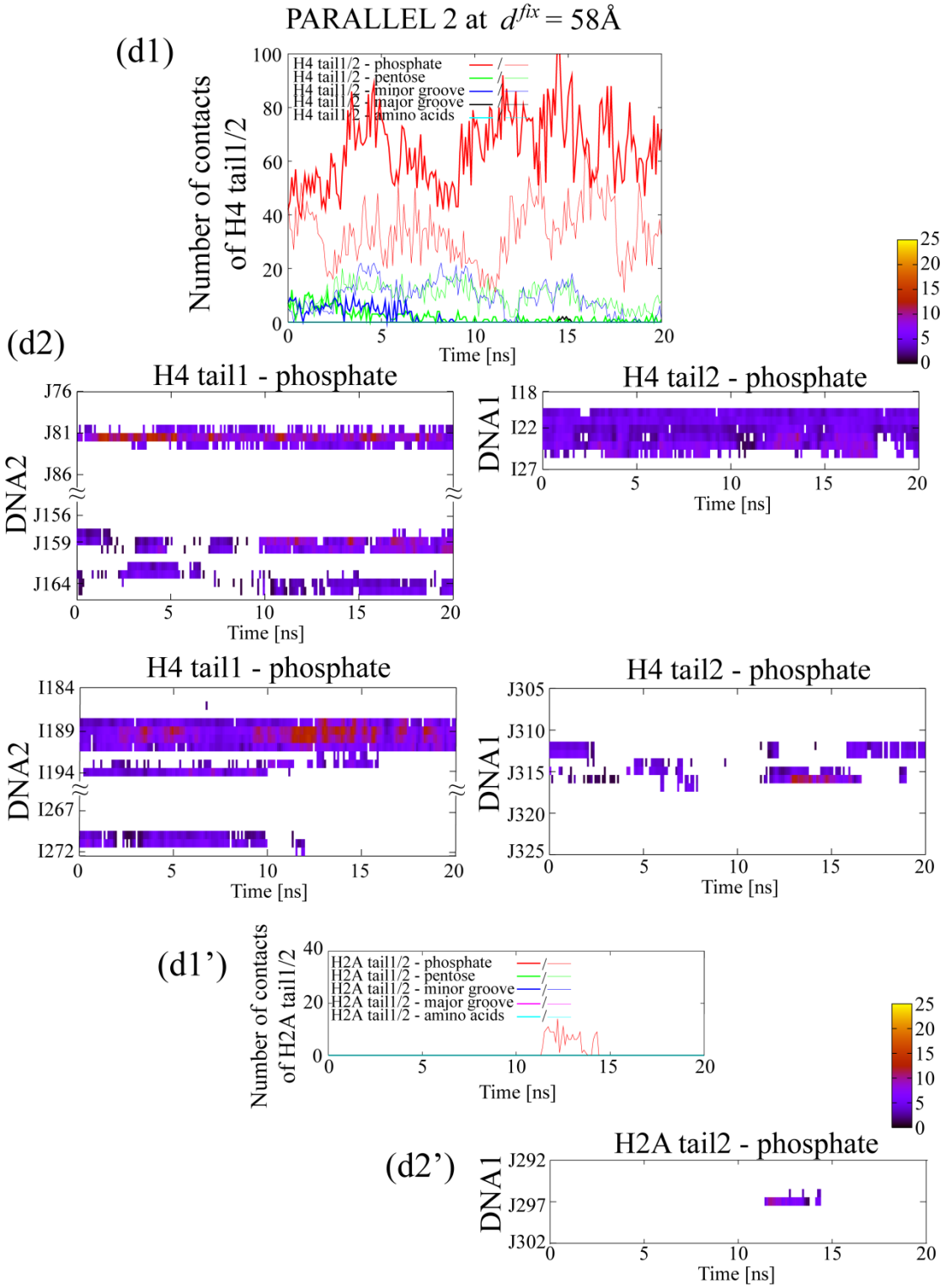
PARALLEL 2 at d^{fix} = 58Å
(d1)
Number of contacts of H4 tail1/2
H4 tail1/2 - phosphate
H4 tail1/2 - pentose
H4 tail1/2 - minor groove
H4 tail1/2 - major groove
H4 tail1/2 - amino acids
Time [ns]
(d2)
H4 tail1 - phosphate
H4 tail2 - phosphate
DNA2
DNA1
J76
J81
J86
J156
J159
J164
I18
I22
I27
I184
I189
I194
I267
I272
J305
J310
J315
J320
J325
Time [ns]
(d1')
Number of contacts of H2A tail1/2
H2A tail1/2 - phosphate
H2A tail1/2 - pentose
H2A tail1/2 - minor groove
H2A tail1/2 - major groove
H2A tail1/2 - amino acids
Time [ns]
(d2')
H2A tail2 - phosphate
DNA1
J292
J297
J302
Time [ns]

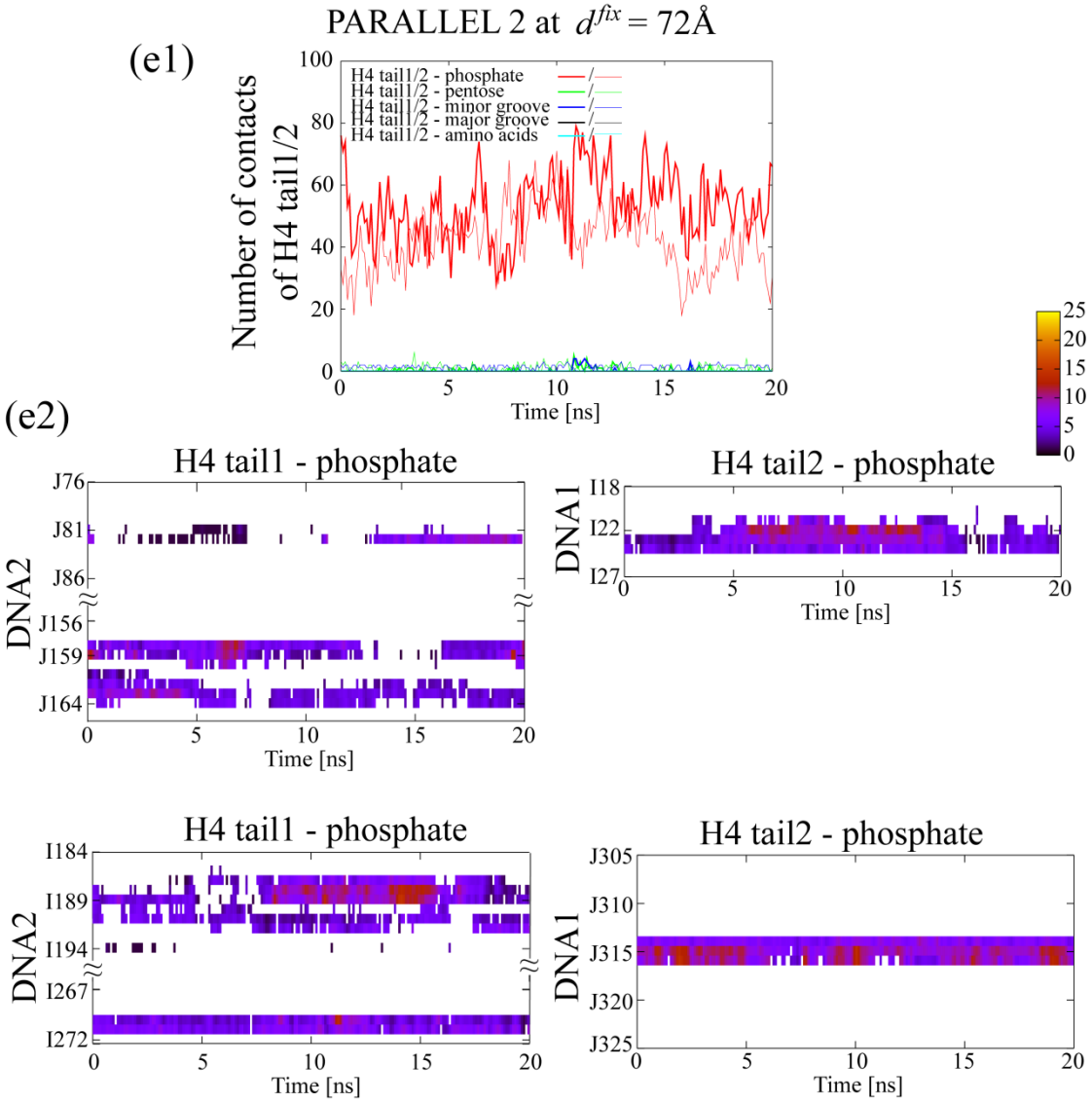
PARALLEL 2 at d^{fix} = 72Å
(e1)
Number of contacts of H4 tail1/2
H4 tail1/2 - phosphate
H4 tail1/2 - pentose
H4 tail1/2 - minor groove
H4 tail1/2 - major groove
H4 tail1/2 - amino acids
Time [ns]
(e2)
H4 tail1 - phosphate
H4 tail2 - phosphate
DNA2
DNA1
J76
J81
J86
J156
J159
J164
I18
I22
I27
H4 tail1 - phosphate
H4 tail2 - phosphate
I184
I189
I194
I267
I272
J305
J310
J315
J320
J325
Time [ns]

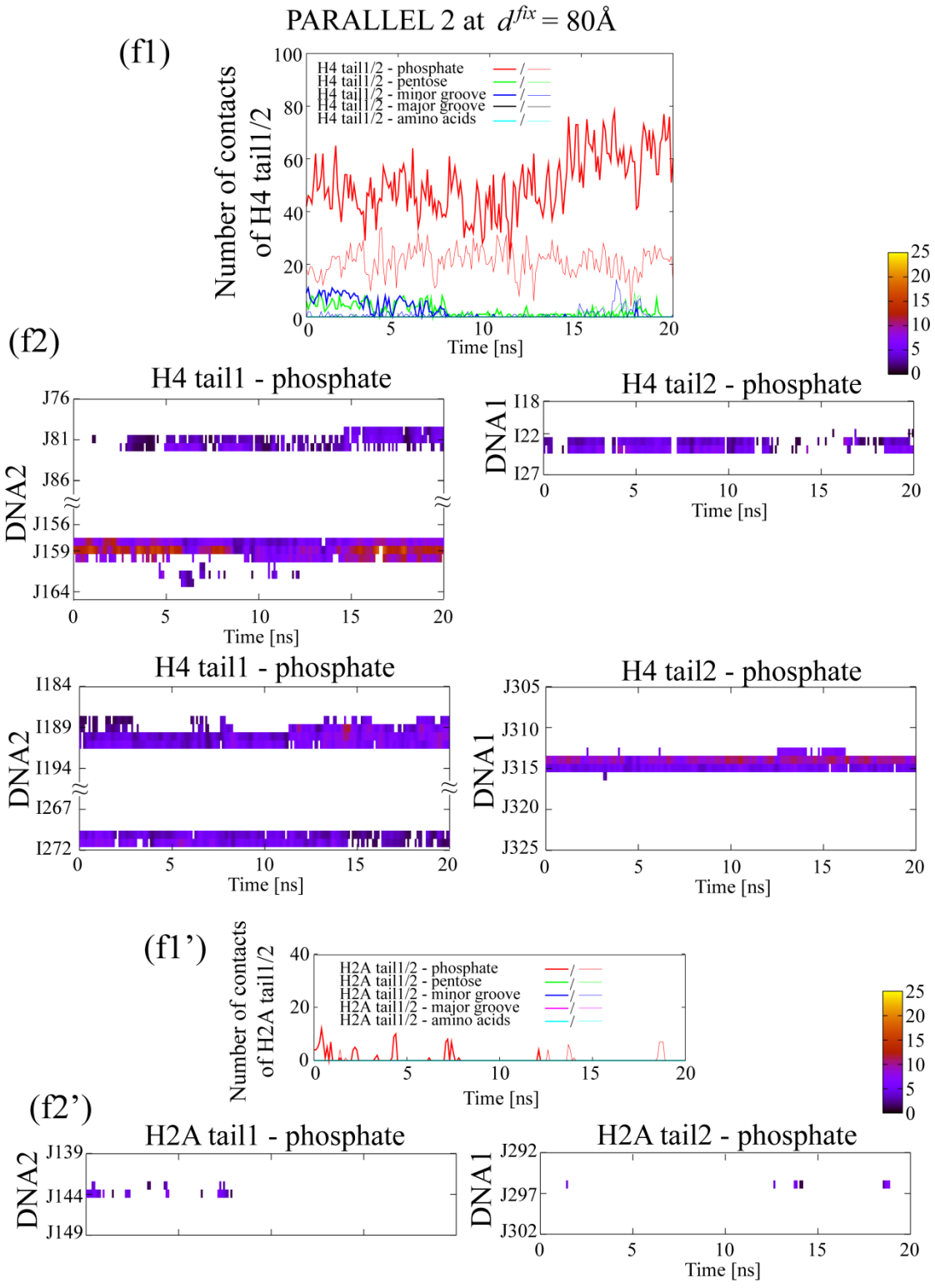

Fig. S9 The number of contacts within 3.5 Å between the (H4 and H2A) tails and the neighboring NCP for the last 20 ns of the umbrella sampling simulation in PARALLEL 1 at (a) d^{fix} = 58 (b) 80 and (c) 98 Å, and PARALLEL 2 at (d) d^{fix} = 58

(e) 72 and (f) 80 Å is shown. To observe the screening effect of the NCP-NCP repulsion, the side-chain atoms of positively charged amino acids, Lys and Arg (Arg3, Lys5, Lys8, Lys12, Lys16, Arg17, Arg19, Lys20, Arg23 in the H4 $tail_{1/2}$, and Arg3, Lys5, Lys9, Arg11, Lys13, Lys15 in H2A $tail_{1/2}$), the atoms of phosphate group (O1P, O2P, O3', O5'), pentose (O4' of the pentose), minor groove (N3 of adenine and guanine, O2 of thymine and cytosine) and major groove (O6 and N7 of guanine, N7 of adenine, O4 of thymine) in the DNA, the side-chain atoms of negatively charged amino acids (Asp and Glu) in the histone octamer were selected for the analysis. The data was analyzed from the trajectory of every 100 ps for the last 20 ns of the umbrella sampling.

The vertical axes in (a1-f1) show the contact numbers of H4 $tail_{1/2}$ and the vertical axes in (a1'), (d1') and (f1') show the contact numbers of the H2A $tail_{1/2}$. The vertical axes in (a2-f2) show the nucleotides in which atoms of the phosphate group interacted with the H4 $tails_{1/2}$, and the vertical axes in (a2'), (d2') and (f2') show the nucleotides in which atoms of the phosphate group interacted with the H2A $tail_{1/2}$. Contact between H2A $tail_{1/2}$ and $DNA_{2/1}$ was not observed at d^{fix} = 80 and 98 Å in PARALLEL 1 and at d^{fix} = 72 Å in PARALLEL 2.

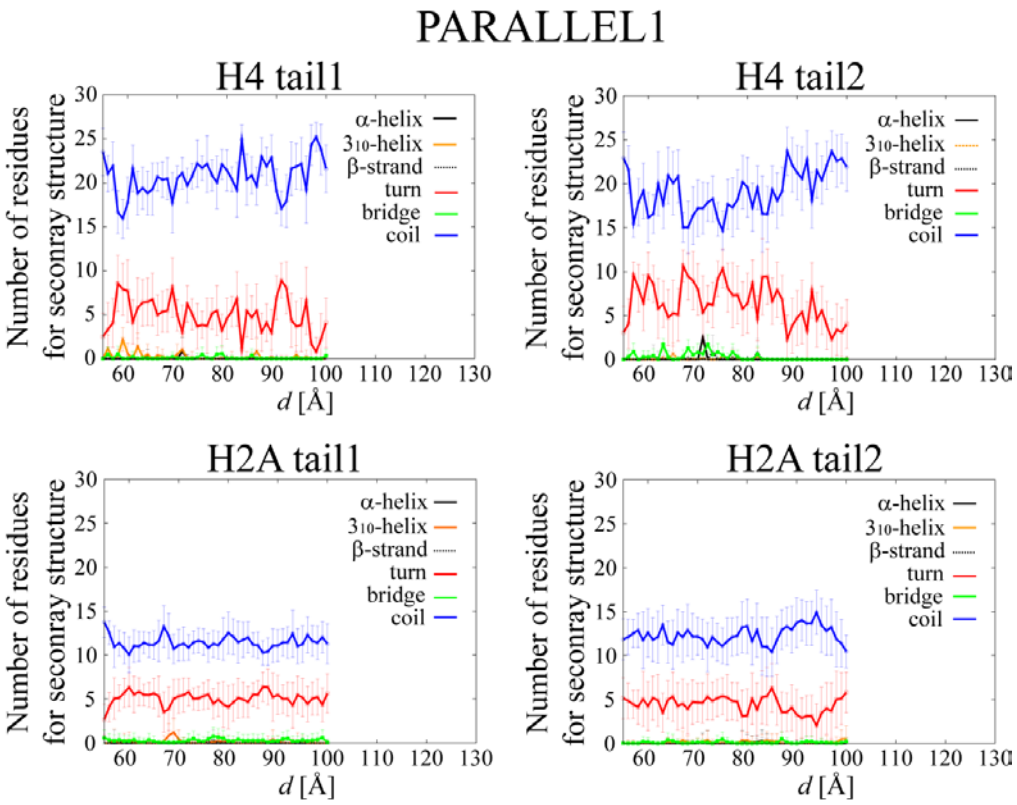

Fig. S10　The average numbers of residues forming α-helix, 3_{10}-helix, β-strand, turn and random coil in the 26 residues in the H4 $tail_{1/2}$ and 17 residues in the H2A $tails_{1/2}$ in PARALLEL 1 are shown against *d*, respectively.　The number of residues forming secondary structures was analyzed using software called STRIDE (19).

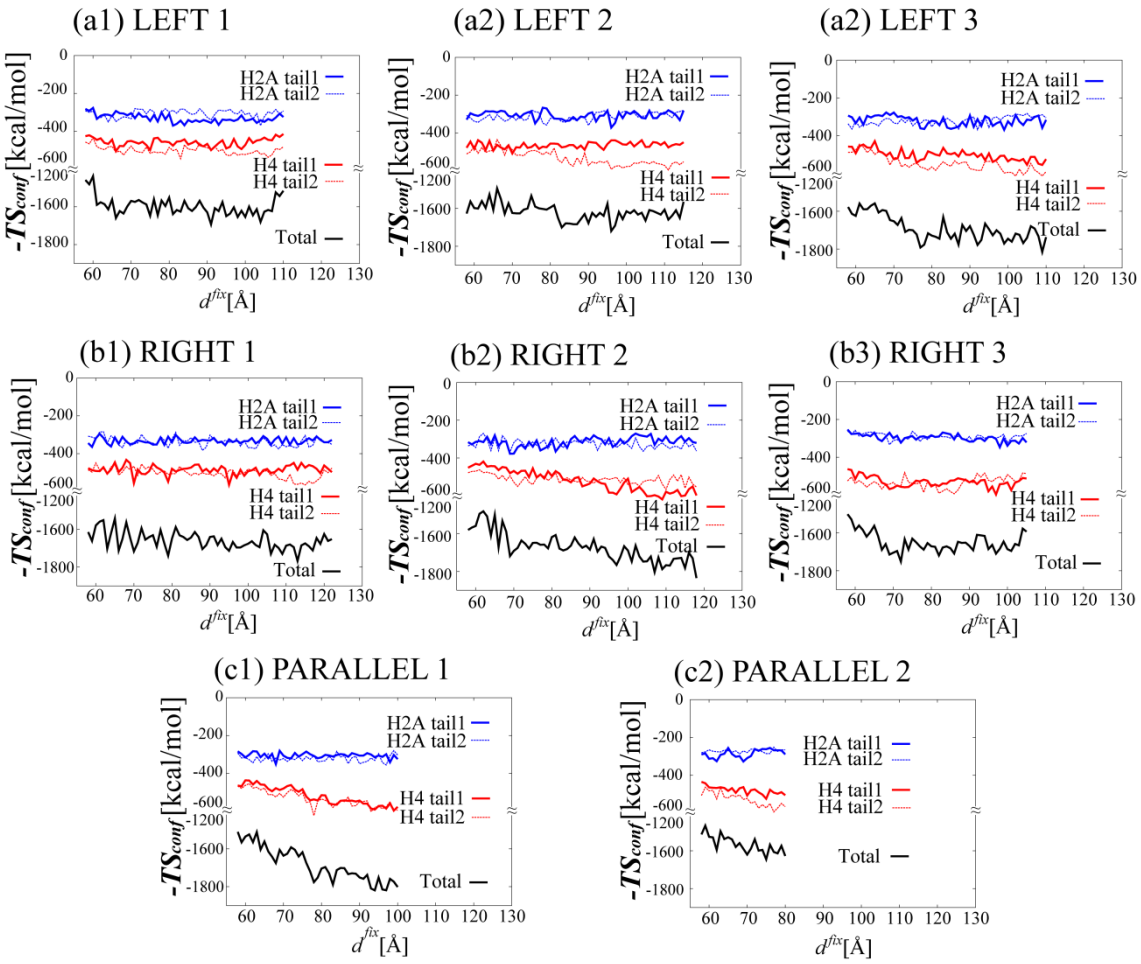

Fig. S11 The conformational entropies of the H4 and H2A tails are shown against d^{fix} in blue and red, respectively. Their total is shown in black.

$-TS_{conf}$ decreased as d^{fix} increased in general. The decrease is clear in LEFT 3, RIGHT 2 and PARALLELs 1-2. However, there were places where $-TS_{conf}$ increased after d^{fix} = ~ 107 Å in RIGHT 1 and after d^{fix} = ~ 90 Å in RIGHT 3. In RIGHT 1, $-TS_{conf}$ of the H4 $tail_1$ increased probably because the H4 $tail_1$ detached from the DNA_2 in the umbrella sampling simulation at d^{fix} = ~ 107 Å during which many conformations were sampled at d = ~ 108 Å, and the detached H4 $tail_1$ stayed on the DNA of its own NCP after d = 108 Å (Fig. S8(b1)). In RIGHT 3, $-TS_{conf}$ of the H4 $tail_2$ increased probably because the H4 $tail_2$ detached from the DNA_1 in the umbrella sampling simulation at d^{fix} = ~ 90 Å during which many conformations were sampled at d = ~ 89 Å, and the detached H4 $tail_2$ stayed on the DNA of its own NCP after d = 89 Å (Fig. S8(b4)).

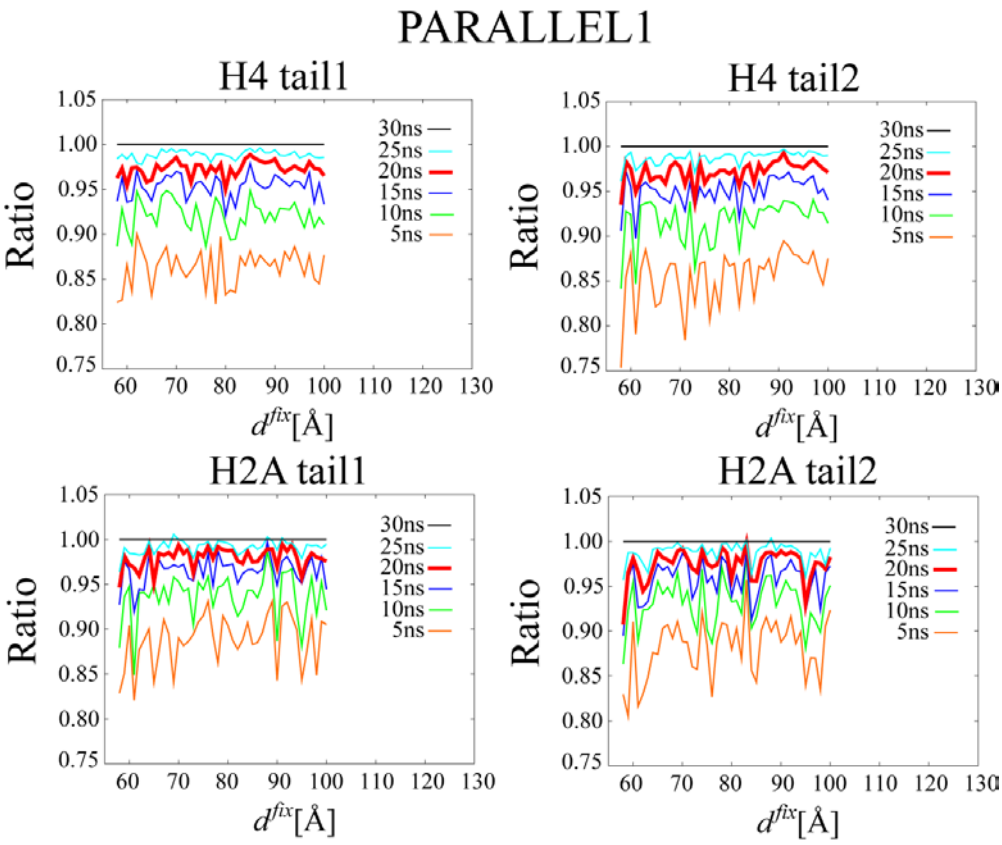

Fig. S12 The convergence for the conformational entropies of the H4 and H2A tails in PARALLEL 1. The ratios of the conformational entropies of the H4 $tail_{1/2}$ and H2A $tail_{1/2}$ for 5 ns (from 10 to 15 ns), 10 ns (from 10 to 20 ns), 15 ns (from 10 to 25 ns), 20 ns (from 10 to 30 ns), 25 ns (from 5 to 30 ns) and 30 ns (from 0 to 30 ns) are shown against those for 30 ns in the umbrella sampling simulations.

Convergence of the conformational entropy of the H2B tails was better than that of the H4 tails probably because the H2B tails are shorter than the H4 tails and the dynamics of the H2B tails were more localized.

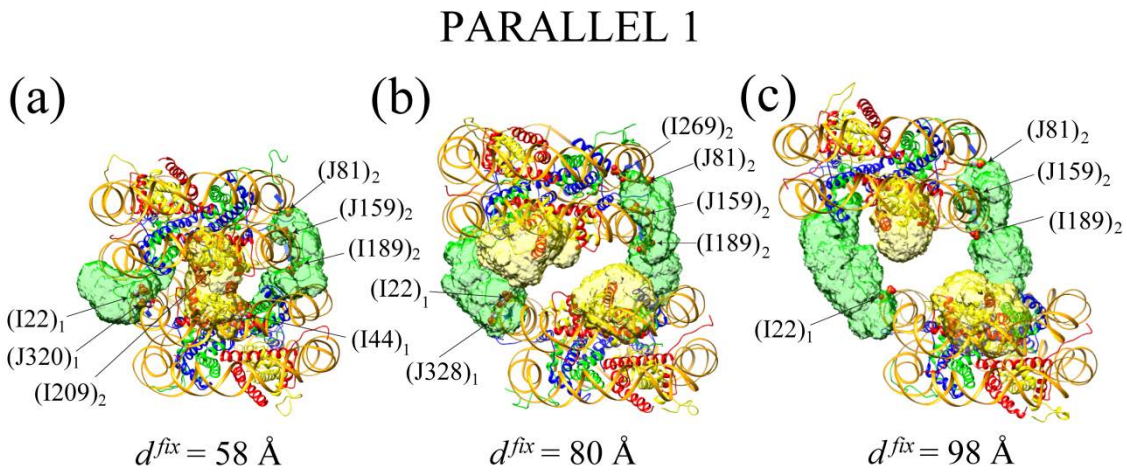

Fig. S13 The spatial distribution of all the atoms in the H4 (in green) and H2A tails (in yellow) in PARALELL 1 at (a) d^{fix} = 58 Å, (b) 80 Å and (c) 98 Å for the last 20 ns of the umbrella sampling simulation. The umbrella sampling simulation at d^{fix} sampled the conformation of the NCPs at d = ~ 58, 80 and 98 Å in Fig. S8(c1). The volumes covered by the atoms in the H4 $tails_{1/2}$ and H2A $tails_{1/2}$ were 14453 / 17517 $Å^3$ and 9637 / 10177 $Å^3$ at d^{fix} = 58 Å, 23140 / 28426 $Å^3$ and 15953 / 20514 $Å^3$ at d^{fix} = 80 Å, 30374 / 31035 $Å^3$ and 23896 / 14977 $Å^3$ at d^{fix} = 98 Å, respectively. To calculate the spatial distribution, the sampled coordinates were located so that the rigid parts of the two NCPs (Gly33−Ala135 of H3, Asn25−Gly102 of H4, Lys15−Thr120 of H2A, and Pro50−Lys125 of H2B histones which were also used to calculate the reaction coordinate) best-fit to the reference coordinate. The initial structure in the *i*-th window of the umbrella sampling simulation was used as the reference coordinate for the best-fit at d_i^{fix}. Some nucleotides in $DNA_{1/2}$ which interacted with Lys and Arg in the H4 and H2A tails are shown in CPK model. The figure was created using Chimera software (20).

For reference, the conformational entropies of the H4 $tails_{1/2}$ and H2A $tails_{1/2}$ were −465.0 / −467.9 kcal/mol and −284.2 / −293.1 kcal/mol at d^{fix} = 58 Å, −516.0 / −536.0 kcal/mol and −315.8 / −336.4 kcal/mol at d^{fix} = 80 Å and −559.1 / −551.3 kcal/mol and −341.8 / −306.8 kcal/mol at d^{fix} = 98 Å, respectively (Fig. S11).

SUPPORTING REFERENCES

1. Ishida, H. and S. Hayward. 2008. Path of Nascent Polypeptide in Exit Tunnel Revealed by Molecular Dynamics Simulation of Ribosome. Biophysical J. 95:5962-5973.
2. Ishida, H. 2010. Branch Migration of Holliday Junction in RuvA Tetramer Complex Studied by Umbrella Sampling Simulation Using a Path-Search Algorithm. J. Comput. Chem. 31:2317-2329.
3. Ishida, H. and A. Matsumoto. 2014. Free-Energy Landscape of Reverse tRNA Translocation through the Ribosome Analyzed by Electron Microscopy Density Maps and Molecular Dynamics Simulations. PLOS ONE 9:e101951.
4. Ishida, H. 2014. Essential function of the N-termini tails of the proteasome for the gating mechanism revealed by molecular dynamics simulations. Proteins 82:1985-1999.
5. Ishida, H. and A. Matsumoto. 2016. Mechanism for verification of mismatched and homoduplex DNAs by nucleotides-bound MutS analyzed by molecular dynamics simulations. Proteins.
6. Hornak, V., R. Abel, A. Okur, B. Strockbine, A. Roitberg, and C. Simmerling. 2006. Comparison of multiple amber force fields and development of improved protein backbone parameters. Proteins 65:712-725.
7. Pérez, A., I. Marchán, D. Svozil, J. Sponer, T. E. Cheatham, C. A. Laughton, and M. Orozco. 2007. Refinement of the AMBER Force Field for Nucleic Acids: Improving the Description of α/γ Conformers. Biophysical J. 92:3817-3829.
8. Joung, I. S. and T. E. Cheatham. 2008. Determination of alkali and halide monovalent ion parameters for use in explicitly solvated biomolecular simulations. J. Phys. Chem. B 112:9020-9041.
9. Jorgensen, W. L., J. Chandrasekhar, J. D. Madura, R. W. Impey, and M. L. Klein. 1983. Comparison of simple potential functions for simulating liquid water. J. Chem. Phys. 79:926-935.
10. Hockney, R. W. and J. W. Eastwood, editors. 1988. Computer simulation using particles: Adam Hilger, New York.
11. Deserno, M. and C. Holm. 1998. How to mesh up Ewald sums. I. A theoretical and numerical comparison of various particle mesh routines. J. Chem. Phys. 109:7678-7693.
12. Ryckaert, J., G. Cicotti, and H. J. C. Berendsen. 1977. Numerical integraton of the Cartesian equations of motion of a system with constraints: molecular

dynamics of *n*-alkanes. J. Comput. Phys. 23:327-341.

13. van Gunsteren, W. F. and H. J. C. Berendsen. 1977. Algorithms for macromolecular dynamics and constraint dynamics. Mol. Phys. 34:1311-1327.
14. Babin, V., C. Roland, and C. Sagui. 2008. Adaptively biased molecular dynamics of free energy calculations. J. Chem. Phys. 128:134101.
15. Raiteri, P., A. Laio, F. L. Gervasio, C. Micheletti, and M. Parrinello. 2006. Efficient Reconstruction of Complex Free Energy Landscapes by Multiple Walkers Metadynamics. J. Phys. Chem. B. 110:3533-3539.
16. Kumar, S., D. Bouzida, R. H. Swendsen, P. A. Kollman, and J. M. Rosenberg. 1992. The weighted histogram analysis method for free energy calculations on biomolecules. I. The method. J. Comput. Chem. 13:1011-1021.
17. Schlitter, J. 1993. Estimation of Absolute and Relative Entropies of Macromolecules Using the Covariance Matrix. Chem. Phys. Lett. 215:617-621.
18. Schalch, T., S. Duda, D. F. Sargent, and T. J. Richmond. 2005. X-ray structure of a tetranucleosome and its implications for the chromatin fibre. Nature 436:138-141.
19. Frishman, D. and P. Argos. 1995. Knowledge-Based Protein Secondary Structure Assignment. Proteins 23:566-579.
20. Pettersen, E. F., T. D. Goddard, C. C. Huang, G. S. Couch, D. M. Greenblatt, E. C. Meng, and T. E. Ferrin. 2004. UCSF Chimera—a visualization system for exploratory research and analysis. J. Comput. Chem. 25:1605.